Liquid-Metal/Water Interactions in a Shock-Tube Geometry

G. Vukovic

August 1991

UWFDM-869

FUSION TECHNOLOGY INSTITUTE

UNIVERSITY OF WISCONSIN

MADISON WISCONSIN

Liquid-Metal/Water Interactions in a Shock-Tube Geometry

G. Vukovic

Fusion Technology Institute
University of Wisconsin
1500 Engineering Drive
Madison, WI 53706

http://fti.neep.wisc.edu

August 1991

UWFDM-869

Liquid-Metal/Water Interactions in a Shock-Tube Geometry

Preliminary Report

by

Gordana Vukovic

Department of Nuclear Engineering and Engineering Physics

University of Wisconsin-Madison

August 1991

Contents

List of Figures

List of Tables

List of Symbols

A — interaction area,

a_{Li} — stoichiometric coefficient of Li,

$a_{\mathrm{H_2O}}$ — stoichiometric coefficient of H_2O,

C_{pd} — molar concentration of liquid metal products,

$C_{\mathrm{H_2O}}$ — molar concentration of H_2O,

C_{Li} — molar concentration of Li,

C_{Limax} — molar concentration of Li in pure $Li_{17}Pb_{83}$,

C_{pd} — molar concentration of liquid metal products,

C_i — molar concentration of species i,

c_{p_i} — specific heat of species i,

c_{f} — sound velocity in fuel,

c_{c} — sound velocity in coolant,

$D_{\mathrm{H_2}}$ — hydrogen production rate proportionality constant,

D_{lm} — liquid metal layer diffusion coefficient.

D_0 — diffusion coefficient proportionality constant,

E_{kin_C} — kinetic energy of coolant,

E_{abs} — absorbed energy,

E_r — reflected energy,

H — enthalpy,

$i_{Li_{17}Pb_{83}}$ — heat of formation of $Li_{17}Pb_{83}$,

$\dot{J}_i$ — molar flowrate of species i,

k_0 — reaction rate coefficient proportionality constant,

k — reaction rate coefficient,

k_{lm} — liquid metal layer thermal conductivity,

l_C — water column height,

M_i — molecular weight of species i,

m — concentration reaction exponent of Li,

m_C — coolant mass,

m_{H_2} — mass of hydrogen,

N_{H_2} — number of moles of hydrogen,

n — concentration reaction exponent of H_2O,

p_{dr} — driving pressure (pressure difference across the diaphragm),

p_{sys} — system pressure (pressure in the driver section),

p_{wh} — water hammer pressure,

R — universal gas constant,

R_{H_2O} — rate at which H_2O is consumed by the reaction,

R_{Li} — rate at which Li is consumed by the reaction,

t — time,

T — absolute temperature,

T_c — coolant temperature,

T_f — fuel temperature,

T_i — contact interface temperature

T_{sn} — spontaneous nucleation temperature,

T_{hn} — homogeneous nucleation temperature.

T_{sat} — saturation temperature,

v — velocity,

v_c — coolant velocity at impact,

ΔE_d — diffusion coefficient activation energy,

ΔE_{H_2} — hydrogen production rate activation energy,,

ΔE_k — reaction rate coefficient activation energy,

ρ — density,

ρ_f — fuel density,

ρ_c — coolant density,

v/o — volume percent.

w/o — weight percent.

Chapter 1

Introduction

The first fusion power reactors will use deuterium and tritium as fuels. In order to be economically feasible, fusion reactors should have blankets containing a tritium breeding material. The ideal blanket material must "a) provide adequate tritium breeding and recovery, b) be compatible with other reactor materials, c) be economically competitive, and d) not cause undue safety and reliability problems."[17]

It is generally assumed that because of its excellent heat-transfer characteristics and good tritium breeding capability, either pure lithium (Li) or some of its compounds or alloys will be used as the "breeding blanket layer and/or primary coolant".[17] In the blanket, lithium will react with neutrons (produced by fusion reactions in the plasma) creating helium and tritium[13]:

$$^{6}\mathrm{Li} + ^{1}n \rightarrow ^{4}\mathrm{He} + ^{3}\mathrm{T} + 4.8\mathrm{MeV} \tag{1.1}$$

After the tritium is removed from the blanket, it will be combined with deuterium and used as a fuel. Materials that are liquid at reactor blanket operating temperatures, such as pure Li and $Li_{17}Pb_{83}$, could serve as tritium breeders and coolant, while solids (e.g. Li_2O, $LiAlO_2$) could serve only as breeders.

Of all its compounds and alloys, Li has the best physical properties and highest breeding capability. But, in designs which intend to incorporate both

liquid lithium and water, there are safety concerns. In some reactor accidents, these materials can come into contact. The Li/H_2O reaction is highly exothermic and self-sustaining. It produces hydrogen (H_2) causing the system to over-pressurize, and if H_2 comes into contact with oxygen, combustion is inevitable. All this also applies to the $Li_{17}Pb_{83}/H_2O$ reaction, with the difference of its relatively benign nature: it is not as exothermic as the Li/H_2O reaction whose severity is a strong function of the contact mode. Therefore, $Li_{17}Pb_{83}$ may be a more suitable material for tritium breeding than Li.

The $Li_{17}Pb_{83}/H_2O$ reaction also raises some safety concerns. This reaction should be completely understood in order to better predict its consequences. Only then can the conceptual fusion reactor designs be improved, so that the likelihood of such a chemical reaction, and its consequences, can be prevented.

Our project is part of the safety studies concerned with the use of liquid $Li_{17}Pb_{83}$ as a reactor blanket and tritium breeder. The purpose of this study is to investigate liquid metal/water interactions in general, and particularly to characterize the chemical kinetics of the liquid $Li_{17}Pb_{83}/H_2O$ interaction through a series of small scale shock-tube experiments, and to develop a model to analyze the experimental results. In these experiments, a water column (driven by argon at high pressure) forcibly impacts a pool of liquid $Li_{17}Pb_{83}$ in the lower portion of the stainless-steel shock tube. The driving pressure and initial H_2O and $Li_{17}Pb_{83}$ temperatures are the parameters of the experiments.

In chapter 2 the physical, chemical, and thermal properties of Li and $Li_{17}Pb_{83}$ are reviewed. In addition, the fuel/coolant interaction and small scale shock-tube experiments are also reviewed. Chapter 3 reviews the previous experimental work of relevance to this proposal. Section 3.2.2 deals with

the physical models used to analyse some of these experiments. In chapter 4 the research goals are stated, and the experimental apparatus (its mechanical design, auxiliary equipment, measurement and data acquisition systems) is described. The experimental procedure and the proposed test matrix are also presented. The results of scoping tests performed on the (largely completed) shock-tube are presented in chapter 5.

Chapter 2

Background

From 1960 until 1980 lithium was considered as the most suitable liquid coolant/tritium-breeding material. At that time, the eutectic lithium-lead alloy, $Li_{17}Pb_{83}$, was proposed as a breeding material in fusion reactors [14]. Subsequently, more data has been gathered on physical and chemical properties, chemical reactivity, heat transfer, and corrosion behavior of lithium-lead.

The advantages of $Li_{17}Pb_{83}$ lie in the fact that it chemically reacts only mildly with air or water, and it can act as a breeder and the neutron multiplier at the same time. Its higher density, higher melting point, (compared to Li) and corrosion behavior with structural materials could be considered as its disadvantages.

In this chapter the main physical, chemical, and thermal properties (of interest for our application) of Li and $Li_{17}Pb_{83}$ will be presented. In addition, processes involved in fuel/coolant interactions (FCI) and the shock-tube contact geometry are briefly discussed.

2.1 Lithium and $Li_{17}Pb_{83}$ Physical, Chemical, and Thermal Properties

In the discussion that follows the major physical, chemical, and thermal properties of Li and $Li_{17}Pb_{83}$ (i.e., those that are of interest for our application) are presented.

Lithium

Li ($^{7}_{3}Li_4$, melting point at 180.54°C, boiling point at 1347°C) belongs to the group of alkali metals. It is silvery and shiny and is the lightest of all metals (its density is about the half that of water). Li has a high electrochemical potential and the highest specific heat of any solid element. It is corrosive and requires special handling[25].

When left in moist air at room temperature lithium does not ignite spontaneously but will slowly oxidize. It reacts with air constituents oxygen, nitrogen, water, and carbon dioxide to form Li_2O (a white powder), Li_3N (a black-violet product), LiOH, H_2, and a small amount of Li_2CO_3, respectively [14].

Lithium reacts with H_2O, generating H_2, and follows one of two reaction paths [17, p.5]:

$$Li + 0.5H_2O \rightarrow 0.5Li_2O + 0.5H_2 + 1.6\times10^5 J/\text{mole Li at } 25°C \quad (2.1)$$

$$Li + H_2O \rightarrow LiOH + 0.5H_2 + 2\times10^5 J/\text{mole Li at } 25°C \quad (2.2)$$

In the first reaction, eq. (2.1), H_2O is the limiting reagent, while in the second one, eq. (2.2), Li is the limiting reagent.

Above the lithium melting point, the Li/air reaction rate becomes large, so that "in normal humidity air, lithium pools spontaneously ignite for temperatures above 243°C. Once ignited, the lithium/air reaction will continue until either the lithium or air is consumed [20]." At increased temperatures the Li/H_2 reaction rate also increases (peaking at 700 °C) so that the reaction could become violent. It should be mentioned here that LiH decomposes at temperatures near 1000°C releasing the H_2 [6, p.37]. Also, it should be kept in mind that the melting point of pure LiOH is 470 °C [6, p.107].

The chemical reactions of Li/H_2O and Li_2O/H_2O at increased temperatures are given in equations (2.3) and (2.4), respectively [6].

$$Li + 0.5H_2O \rightarrow 0.5Li_2O + 0.5H_2 + 3.6\times10^5 \text{ J/mole Li at } 685°C \quad (2.3)$$

$$Li_2O + H_2O \rightarrow 2LiOH + 6.9\times10^4 \text{ J/mole } Li_2O \text{ at } 850°C \quad (2.4)$$

$Li_{17}Pb_{83}$

One lithium alloy of interest is the eutectic $Li_{17}Pb_{83}$. The equilibrium phase diagram of Li-Pb system is given in figure 2.1, while table 2.1 contains its main physical and thermal properties [2,14].

In references terms "modest", "mild", and "slow" are qualitatively used to describe the reaction of $Li_{17}Pb_{83}$ with water. This reaction, as in case of Li/H_2O reaction, can follow one of the two reaction paths:

$$Li_{17}Pb_{83} + 8.5H_2O \rightarrow 8.5Li_2O + 8.5H_2 + 83Pb + Q_1 \quad (2.5)$$

$$Li_{17}Pb_{83} + 17H_2O \rightarrow 17LiOH + 8.5H_2 + 83Pb + Q_2 \quad (2.6)$$

Including the heat of formation of $Li_{17}Pb_{83}$ ($i_{Li_{17}Pb_{83}} = 8242$J/mole $Li_{17}Pb_{83}$

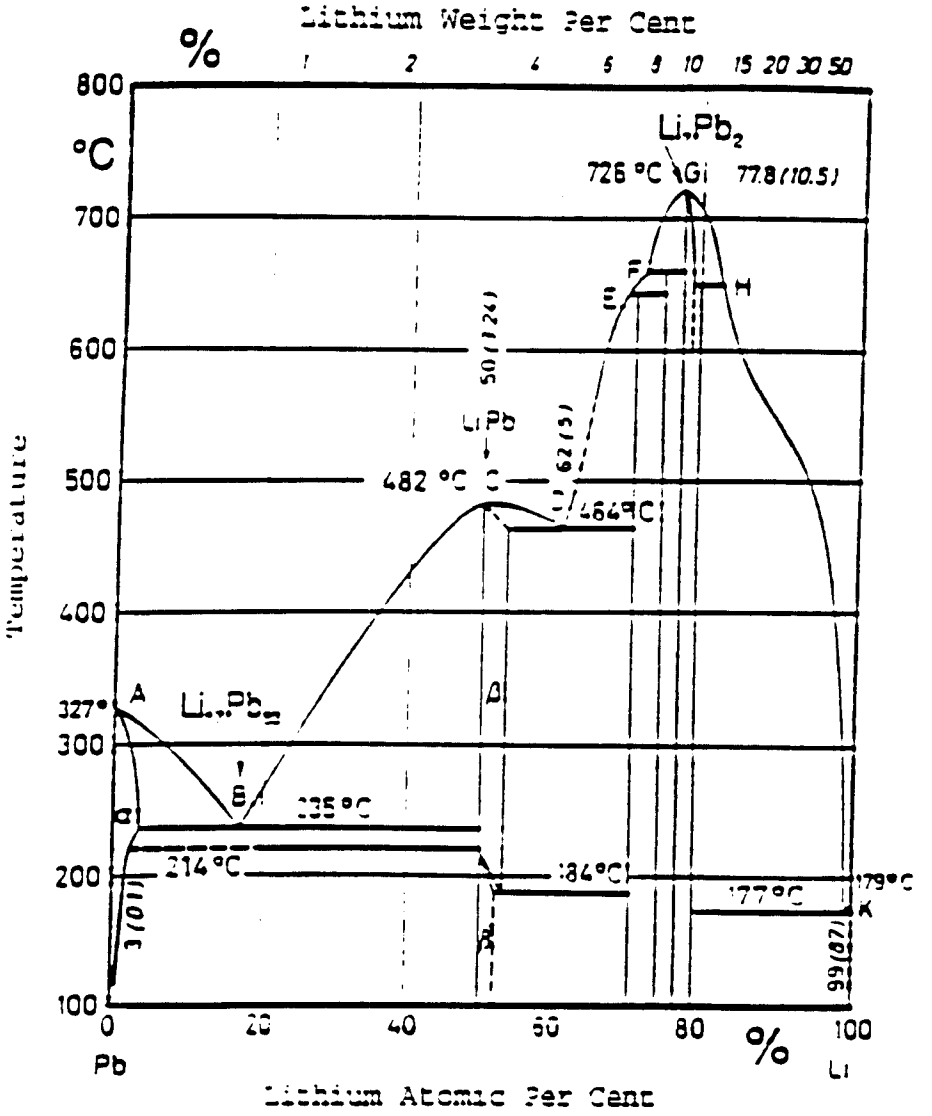

Figure 2.1: Equilibrium phase diagram of Li-Pb system [13]

Property	Value
molecular weight [g/mole]	173.16
lithium content [g/cm^3]	0.065 ($0.68w/o$ or $12.7v/o$ of Li)
density [kg/m^3]	$\rho = 9495 - 0.695(T - 508)$, $508K < T < 873K$
melting point (temperature of fusion) [°C]	234.75
latent heat of fusion [J/g]	29.59
thermal conductivity[a] [W/(Km)]	$k = 8.627 + 0.0205T$, $508K < T < 873K$
specific heat at constant pressure[b] [J/(kg)]	$c_{ps} = 0.1458 - 2.087\times10^4T + 6.029\times10^7T^2$, for 298K$< T < T_{fus}$, $c_{pl} = 0.6271 - 7.908\times10^4T$, for $T_{fus} < T <$573K

[a]Given equation is a linear fit through the values calculated from those of pure elements.
[b]c_{ps} and c_{pl} are the specific heats of the alloy in solid and liquid state.

Table 2.1: $Li_{17}Pb_{83}$ properties [2,14].

[8, p.14]), the values of heats of reactions at 25°C are $Q_1 = 1.896 \times 10^4$J/mole $Li_{17}Pb_{83}$ and $Q_2 = 2.576 \times 10^4$J/mole $Li_{17}Pb_{83}$.

What reaction will take place depends on the mass ratio of the reactants. The first reaction, eq. (2.5), is H_2O limited, while the second reaction, eq. (2.6), is Li limited. Hydrogen produced in these reactions is soluble in $Li_{17}Pb_{83}$, but its solubility in $Li_{17}Pb_{83}$ is orders of magnitude lower than its solubility in lithium [20].

The lower hydrogen flammability limit is $4v/o$ and, depending on the volumes of $Li_{17}Pb_{83}$ and air, the hydrogen concentration could reach the lower hydrogen flammability limit. In the worst case, if there is a spark in a reaction vessel, a large-scale $Li_{17}Pb_{83}/H_2O$ reaction could lead to hydrogen combustion [20].

Piet et al.[20] have summarized the existing results of $Li_{17}Pb_{83}$-gas tests. According to them "$Li_{17}Pb_{83}$ is not expected to ignite in air for $Li_{17}Pb_{83}$ temperatures through 1000°C. However, some aerosols are observed at 700°C and more would be expected at higher temperatures. The low severity of the $Li_{17}Pb_{83}$-air reaction apparently comes from (a) the low amount of lithium in $Li_{17}Pb_{83}$ (0.68% by mass), (b) ability of the lead to act as a heat sink, and/or (c) the lithium becoming depleted near the $Li_{17}Pb_{83}$ surface, allowing lead to hinder further lithium diffusion to the surface. $Li_{17}Pb_{83}$/air or $Li_{17}Pb_{83}/N_2$ reactions do not appear capable of causing significant temperature increases. However, a $Li_{17}Pb_{83}/CO_2$ reaction test did show a rapid temperature increases from 454°C to 645°C at which point the CO_2 was consumed."[20, p.280] The reaction of eutectic $Li_{17}Pb_{83}$ with nitrogen from air is limited to a very thin surface layer which can be easily rubbed off. It was shown that $Li_{17}Pb_{83}$ also

reacts mildly with concrete producing H_2.

The major observations regarding the $Li_{17}Pb_{83}$ application in fusion reactor designs are summarized bellow:

- "At operating temperatures of many proposed fusion reactor blankets, $Li_{17}Pb_{83}$ is highly fluid and thermally conductive, has high cross sections for fast and thermal neutrons, and provides an adequate breeding ratio." [6, p.2]

- $Li_{17}Pb_{83}$ can be used as both breeder or coolant, or can be cooled by water.

- If $Li_{17}Pb_{83}$ is considered as a breeder then austenitic stainless steels (mainly AISI 316), ferritic stainless steels, and vanadium should be considered as promising blanket structural materials.

- From the safety standpoint the water cooling should be eliminated from the building that contains either lithium or $Li_{17}Pb_{83}$ [20, p.273][1].

The last of the above conclusions is based on an incomplete knowledge of the kinetics of the molten $Li_{17}Pb_{83}/H_2O$ chemical reaction. The main goal of this project is to understand in greater detail the kinetics of that chemical reaction. This understanding should enable the designers utilizing molten metal and water in engineering systems to reduce both the likelihood of an accident and its consequences.

[1] Lomperski, Krueger, Corradini, the Madison Fire Department, and all the inhabitants of ERB strongly agree.

2.2 Fuel/Coolant Interaction and Small Scale Shock-Tube Experiments

Liquid metal (LM)/water interactions belong to the broader category of fuel/coolant interactions (FCI). A FCI occurs when a hot liquid (fuel) comes into contact with a colder more volatile liquid (coolant). This results in vigorous boiling of the coolant caused by rapid fuel fragmentation. This boiling-fragmentation process can lead to high local vapor pressures which if not relieved can lead to a physical explosion.

The following liquid metal/water contact modes are possible: injection (water into liquid metal), pouring [2] (liquid metal into water), layered (liquid metal and water come into contact as stratified layers), a pool ("steam environment over liquid metal pool"[20, p285]), and a spray ("steam environment present during liquid metal spray"[20, p285]). The coolant injection (fig. 2.2) would occur after, for example, "a tube rupture in a liquid metal steam generator or in a pressurized blanket module"[6, p.4]. Due to a reactor accident, blanket compounds could rupture, causing the liquid metal to pour onto a pool of water (fig. 2.3). In the case that the water and breeder-blanket tubes in the vacuum vessel rupture (again, due to an accident), these reactants will spray into a common volume — spray contact mode (fig. 2.4)[6].

[2] "Interestingly, $Li_{17}Pb_{83}$ is about ten times more dense than water, but water is twice as dense as lithium. Thus, $Li_{17}Pb_{83}$ will pour through a water pool, while lithium poured on top of water tends to float on top of the water. Conversely, water tends to pour through a lithium pool, while water poured on top of $Li_{17}Pb_{83}$ will form a layer on top of the $Li_{17}Pb_{83}$. The distinction between pouring through and forming a stratified layer on top may be important because the pouring contact mode may entail more mixing between liquid metal and water, hence more reaction. Note, the layered mode is somewhat idealistic; in reality at relevant temperatures, vapor explosions and turbulent mixing may prevent layering."[20, p.285]

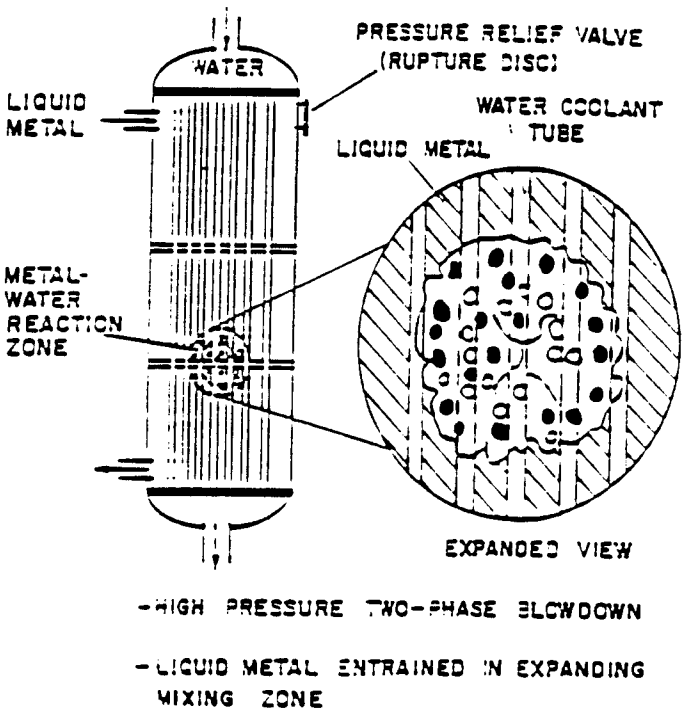

Figure 2.2: Coolant injection contact mode [6].

The purpose of this work is to study the impact of a water column on a layer of molten metal (e.g., $Li_{17}Pb_{83}$) under carefully controlled, repeatable conditions. This contact geometry is a special case of the stratified situation where the two liquids are forcibly mixed. A small scale (small contact area) shock-tube experiment is an appropriate choice for our studies. The shock-tube geometry can be considered as a one-dimensional unit cell of a stratified geometry, in which one can control the vapor film collapse process. This assumption simplifies the theoretical analysis and allows various experimental parameters to be studied separately with maximum control over the initial conditions.

In the following subsections, the shock-tube basic design, together with the processes involved in liquid metal/water shock-tube experiments, will be

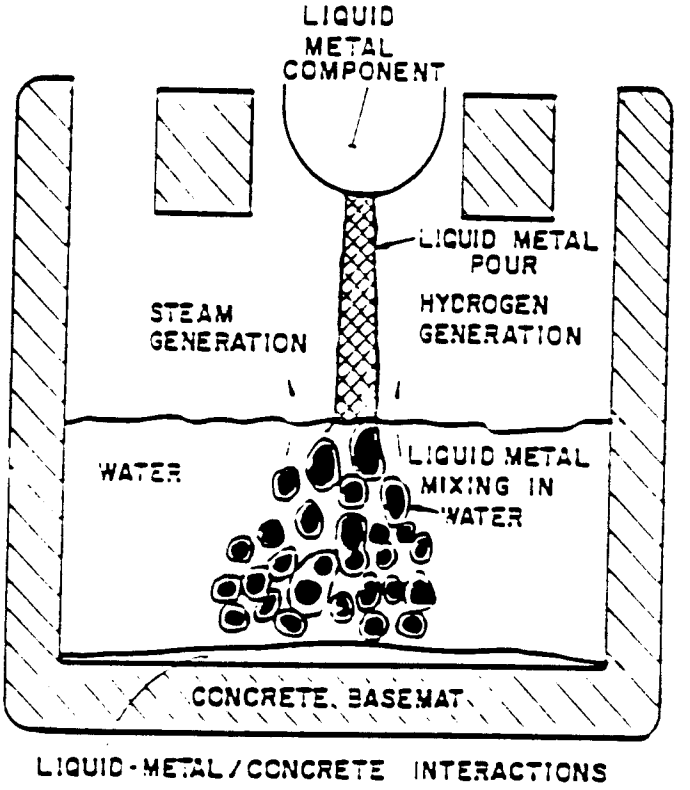

Figure 2.3: Liquid metal pouring contact mode [6].

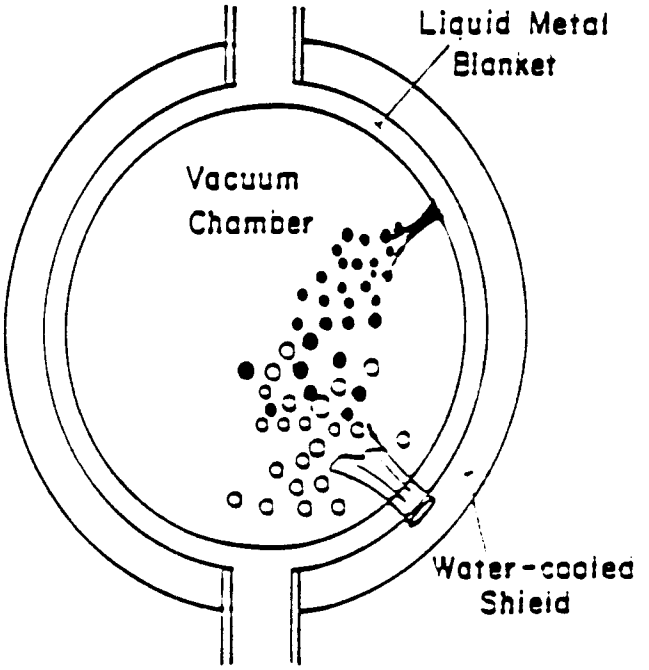

Figure 2.4: Spray contact mode[6].

given.

2.2.1 Liquid Shock-Tube — Basic Concept

The main parts of a shock tube are the driver section (DS) and the reaction tube (RT) separated by the rupture diaphragm[3] (in most cases). The reaction tube is filled with the fuel (i.e., molten metal), while the space between the diaphragm and fuel surface is usually either under the vacuum or filled with a vapor or some inert gas. The driver section is filled with coolant driven by a cover gas at some desired pressure.

[3]The rupture diaphragm will be referred to as the diaphragm.

2.2.2 Qualitative Description of Shock-Tube Experiments

The rapid fuel/coolant heat transfer, vapor generation, and mechanical energy release are the major processes involved in liquid metal/water interaction as shown by previous shock-tube experiments([6,12]).

At the moment when the diaphragm breaks, the water column, driven by the gas in the driver section, impacts the melt surface, and mixes with the fuel[4]. The initial pressure difference across the diaphragm (driving pressure) defines the initial kinetic energy of the impacting water column. A part of that energy is absorbed by the fuel and is used for fuel fragmentation and fuel-coolant mixing, while the rest of energy is reflected from the water surface. As a result, the fuel becomes dispersed in the coolant, providing a large surface area and allowing rapid heat transfer. This combination of hydrodynamic impact and thermal interaction generates coolant vapor and high pressure pulses. The compression/rarefaction pattern lasts until the heat of the melt (i.e., heat for vapor generation) is exhausted. If the heat transfer is extremely fast (as in experiments with high initial liquid metal temperatures and driving pressures) a vapor explosion is possible.

In some of our experiments (e.g. $Li_{17}Pb_{83}/H_2O$ interaction) in addition to rapid heat transfer and mechanical energy release, we will have a liquid metal/water chemical reaction with the production of hydrogen. The hydrogen produced, together with the water vapor, will give rise to the pressure in the shock-tube. Since the $Li_{17}Pb_{83}/H_2O$ reaction is mainly a surface reaction [11],

[4] "This contact mode is similar to water(l) injection since the water is forcibly introduced and mixed with the liquid metal."[20, p.287]

the amount of H_2 produced will depend, among the other parameters, on the contact area.

Chapter 3

Previous Experimental Investigations

In the past, fuel/coolant interaction experiments were performed in one of the following three contacting modes: free-contacting (or dropping i.e. pouring) mode, injection mode, and shock-tube mode [23]. This review is oriented only to liquid metal/water interactions in the shock tube geometry. The other contact modes are described widely in the literature and the reader interested in those is referred to references [17,10,20,6].

Past liquid metal/water interaction experiments are described in the first part of this chapter. Section 3.2 contains the most recent lithium and lithium alloys/water interaction experiments directly related to our research goals.

3.1 Past Investigations

Table 3.1 summarizes the main parameters of past experiments of interest for our work. Their results are discussed further in this section.

Hillary et al.[9] In order to examine the influences of the system pressure (i.e.. pressure in the driver section), the pressure below the diaphragm, and the fuel temperature, Hillary et al. have done experiments with water as a coolant and molten lead or molten salt mixtures (i.e., mixtures of lithium and

Reference		Hillary et al. [9]	Darby et al. [4]	Segev et al. [22]	Kottowski and Grossi [11]
System		Water/Molten Lead	a)Water/ Molten Aluminum b)Water/ Molten Lead	Water/Wood's metal[a]	a)Water/ Molten Lead b)Water/ $Li_{17}Pb_{83}$
Coolant Temp.[°C]		...	20	...	25
Fuel Temp.[°C]		370–510	a)725 b)473–820	...	470
System Pressure [10^5Pa]		2–3	...	25.4	1–25
Pressure Bellow Diaphragm [Pa]		0.13–1300	a)18mmHg b)...	1.6	0.1
Driver	Diameter[mm]	20	25.4	25.4	9
Section	Length[m]	1.6	3 feet	1.6	2
	Water Column Length[m]	1.36–1.59	0.84	...	2.1
	Cover Gas	helium	...	argon	argon
Reaction	Diameter[mm]	20	25.4	25.4	20
Chamber	Length[m]	0.25–0.30	...	0.117	0.08
	Cover Gas	water vapor; inert gas; vacuum	a)water vapor, argon, vacuum b)water vapor, vacuum	water vapor; inert gas; vacuum	vacuum
Pressure Spikes	Maximum Pressure [10^5Pa]	34 –71	a)255–304 b)...	...	a)12–250 b)8–174
	Number of Pulses	several (in most cases)	several	several (in most cases)	a)one for p_{dr}=1bar and several for higher driving pressure b)one

[a]50% Bi, 25% Pb, 12.5%Cd, and 12.5% Sn

Table 3.1: Past experiments — parameters

potassium chlorides) as a fuel. Their apparatus consisted of a stainless steel driver section and a transparent silica reaction tube. The distance between the water column (usually 1500mm high) and the hot liquid (usually 60mm deep) was 150–200mm. Before the initialization of the experiment, that space was either evacuated or filled with water vapor or some non-condensible gas (e.g. argon). Two quartz piezo-electric pressure transducers were used to record pressure changes and the interaction was observed and recorded for approximately 1sec by high speed photography techniques.

Their results have shown that high shock pressures are generated in this kind of experiment The observed pressure spikes were lower than water-hammer pressures. Thermal to mechanical energy conversion efficiency was quite low. A limited depth of fuel was involved in the reaction, so that the energy that could have been transferred to the water was also limited. Each fuel/coolant contact resulted in mechanical energy release (manifested as water column bouncing) and an additional amount of lead was carried up the tube by the steam-driven water. The behavior was almost identical in a test with water and molten salt mixture "indicating a marginal effect of relative density on the depth of the mixing zone"[9, p.857]. When an inert noncondensible gas was present in the space separating the two liquids the bouncing after impact was completely eliminated and the deformation of the lead was greatly reduced.

In order to examine the effect of varying the hot lead temperature through the water critical temperature(374°C), three experiments were carried out, but there were no obvious effects on the generated pressure.

Darby et al.[4] have performed a number of small scale shock-tube experiments to study the thermal interaction between water and molten aluminum. The upper part of the apparatus was made of stainless steel. It contained the water column 84cm high, supported by a stretched rubber diaphragm. The molten aluminum was contained in a steel crucible. During the experiment the pressure history at eight points along the upper part of the shock tube was recorded using piezo-electric pressure transducers. The surface area and the size distribution of the aluminum debris have been measured after the experiment.

A series of introductory experiments was performed to understand the dynamics of the process. In order to photograph the motion of the water surface before impact, a transparent quartz tube was used instead of the metal crucible. Unfortunately, the quartz tube could stand only the experiments with cold aluminum. When the region between the diaphragm and the metal surface was under vacuum prior to impact, the violent flashing of the water front surface was observed. The flashing was eliminated by introducing water vapor of the pressure corresponding to the water temperature.

The maximum pressure pulse in their heated water/molten Al experiments (performed in the all steel rig) was usually produced on the second bounce impact of the series of impacts in each experiment. In most cases the pulse had a small initial rise and a plateau, and then a rapid rise (200μsec) to its maximum value. After a slow decay ($\sim$2msec) the pressure would fall to its initial value. The aluminum debris was highly fragmented and made up of agglomerates of small particles. The experiments with the highest pressure pulses gave the most finely divided debris. The presence of argon in the space

between the diaphragm and fuel had an inhibiting effect on the interaction.

The volume of molten lead used in their water/molten lead experiments was the same as in the aluminum tests. But, the peak pressures were barely greater than the theoretical impact pressures and the debris was far less fragmented than in the water/molten aluminum experiments. However, the results compare well with those given in [9].

Segev et al.[22] The effects of the liquid physical and chemical properties, temperatures of the fuel, and initial system pressure were evaluated by Segev et al. Three regions were observed. When the fuel temperature, T_f, was lower than the spontaneous nucleation temperature, T_{sn}[1] , no thermal interaction occurred and the coolant column bounced only if vapor was initially present. The maximum impulse always occurred on the first impact. Pressure pulses on the order of the theoretical water hammer pressure, p_{wh}, were produced in cases when $T_f > T_{sn}$ and the contact interface temperature, T_i, was less than T_{sn}. In all runs the maximum pressure pulse occurred on the second, third, or fourth bounce, but never on the first one. Experiments where $T_i > T_{sn}$ were characterized by fast vaporization and pressure pulses larger than p_{wh}. The maximum impulse never occurred on the first impact. Experiments in

[1] Homogeneous nucleation is a process of vapor formation in a metastable liquid where the size of the equilibrium vapor nucleus (r^*) is equal to the liquid molecular dimension. "... bubbles smaller than r^* will collapse and bubbles larger than r^* will grow spontaneously.[3, p.114]" The corresponding temperature is called 'homogeneous nucleation temperature', T_{hn}. In presence of a flat surface, depending on whether the particular liquid in question wets the surface (and how much) or not, the liquid superheat requirement, $T - T_{sat}$(where T is the liquid temperature and T_{sat} is the liquid saturation temperature), can be reduced or not, and the corresponding superheated liquid temperature is called the "spontaneous nucleation temperature", T_{sn}. In the case when the liquid completely wets the surface there is no reduction in the superheat and $T_{sn} = T_{hn}$. In the case when the surface is non-wetting no superheat is required for the nucleation at the surface and $T_{sn} = T_{sat}$.

region where $T_i > T_{sn}$ were also done at elevated pressures (i.e. with larger driving pressures). They showed that the number of bounces was reduced (two or three only), pressure pulses were of lower magnitude and with longer rise time compared to the low driving pressure data. This suggested that slow vaporization occurred instead of an explosive thermal interaction.

Kottowski and Grossi[11] Since the main purpose of their experiments was to check the influence of the chemical reactivity on the liquid metal/water interaction, the $Li_{17}Pb_{83}$ experiments were duplicated with Pb melt (initial fuel and coolant temperatures were the same for all experiments; the only variable was the driving pressure). It was found that the energetics of the fuel/coolant interaction depends only on the degree of mixing and fragmentation at the beginning of the interaction. In cases when the system pressure was $\geq$5bar the pressure trace for the Pb/H_2O system had several spikes (the second one being largest), while in $Li_{17}Pb_{83}$ experiments neither peaky impact pressures nor repeated ejections and reentries were observed. These experiments have clearly shown that the chemical reaction (i.e. the noncondensible gas, H_2, production) cushions the impact, attenuating greatly the effect of mixing and fuel fragmentation.

The investigations described in this section have helped us to define the relevant parameters (initial fuel and coolant temperatures, initial system pressure and the pressure below the rupture disc, and the gas below the diaphragm) for our future experiments. The review of their experimental apparatus were an excellent source of ideas for the mechanical design of our shock tube.

3.2 Recent $Li_{17}Pb_{83}/H_2O$ Experiments

The data base on $Li_{17}Pb_{83}/H_2O$ reactions done in a shock-tube geometry is rather small. The two most recent small-scale experiments done for initial parameters in ranges of interest for our work will be described in this section.

3.2.1 Experimental Designs

Herzog [6] has performed a series of small scale $Li_{17}Pb_{83}/H_2O$ interaction experiments to determine the hydrogen production rate (i.e. the chemical kinetics) in pouring experiments (more precisely, he has dealt with fuel/coolant interaction with the stratified layer contact mode) performed under different initial conditions (initial liquid metal and coolant temperatures). He has also developed two physical models (Kinetic Reaction Rate and Liquid Metal Transport Reaction model, described in section 3.2.2) in order to analyze the collected data. The experiments were performed in a closed vessel at $\sim$ 1bar (the scheme of the experimental set-up is given in fig. 3.1). A closed system was chosen so that by measuring the system pressure, gas and water temperatures, and by knowing the initial conditions the hydrogen production during the reaction could be determined. When the butterfly valve opens, water (roughly 1 liter) from the upper portion (50.8mm I.D.) of the reaction vessel pours on top of the molten $Li_{17}Pb_{83}$ (its mass was in the range from 20 g up to 65 g) contained in the lower liquid metal pool (25.4mm I.D.). The reaction was recorded for 200sec and it was accompanied by H_2 production.

The experimental data have shown that the extent of the reaction did not depend on the water temperature. In fig. 3.2, the mass of H_2 at 200sec is shown

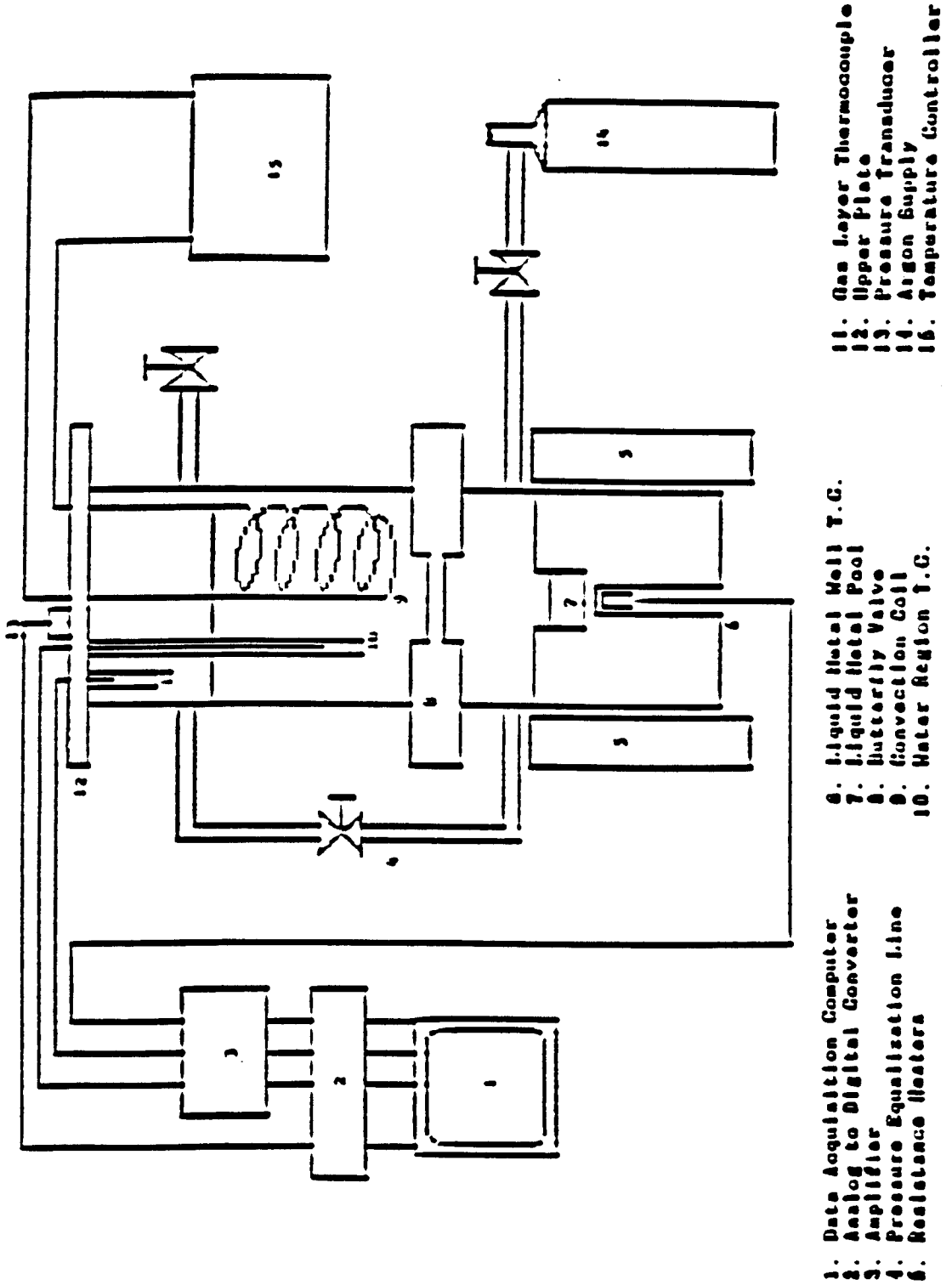

Figure 3.1: Herzog's closed vessel experiment [6, p.44].

as a function of the initial liquid metal temperature. The data shows that the extent of the reaction depends on the initial liquid metal temperature. Its maximum (occurring at a liquid metal temperature of $\sim$ 400°C) was explained by the phase transition of LiOH (reaction product)[7].

Herzog experienced several problems while running his experiments. Among them were the following:

- since the gas layer and water thermocouples were placed in thick-walled thermocouple wells, their response times were quite long. As a consequence, the hydrogen partial pressure evolution during the early time of the reaction could not be calculated easily.
- The whole system was slowly leaking during the experiment, and that had to be taken into account in data analysis.

Lomperski [16] first modified Herzog's apparatus to correct these deficiencies and than performed additional experiments (for initial liquid metal temperatures higher than 420°C). Among the numerous improvements that he made was the redesign of gas temperature measurements. He succeeded to measure the gas temperature with a bare (much faster) thermocouple. Lomperski's experimental data is presented in fig. 3.3.

Lomperski's and Herzog's data are of the same order of magnitude. Only those values of H_2 mass measured for initial liquid metal temperature of $\sim$ 400°C (i.e. 400°C in fig. 3.2 and at $\sim$ 423°C in fig. 3.3) differ by a substantial amount. More data points in that region (i.e. for initial liquid metal temperature in the 350–500°C range) are needed before any final conclusions can be made.

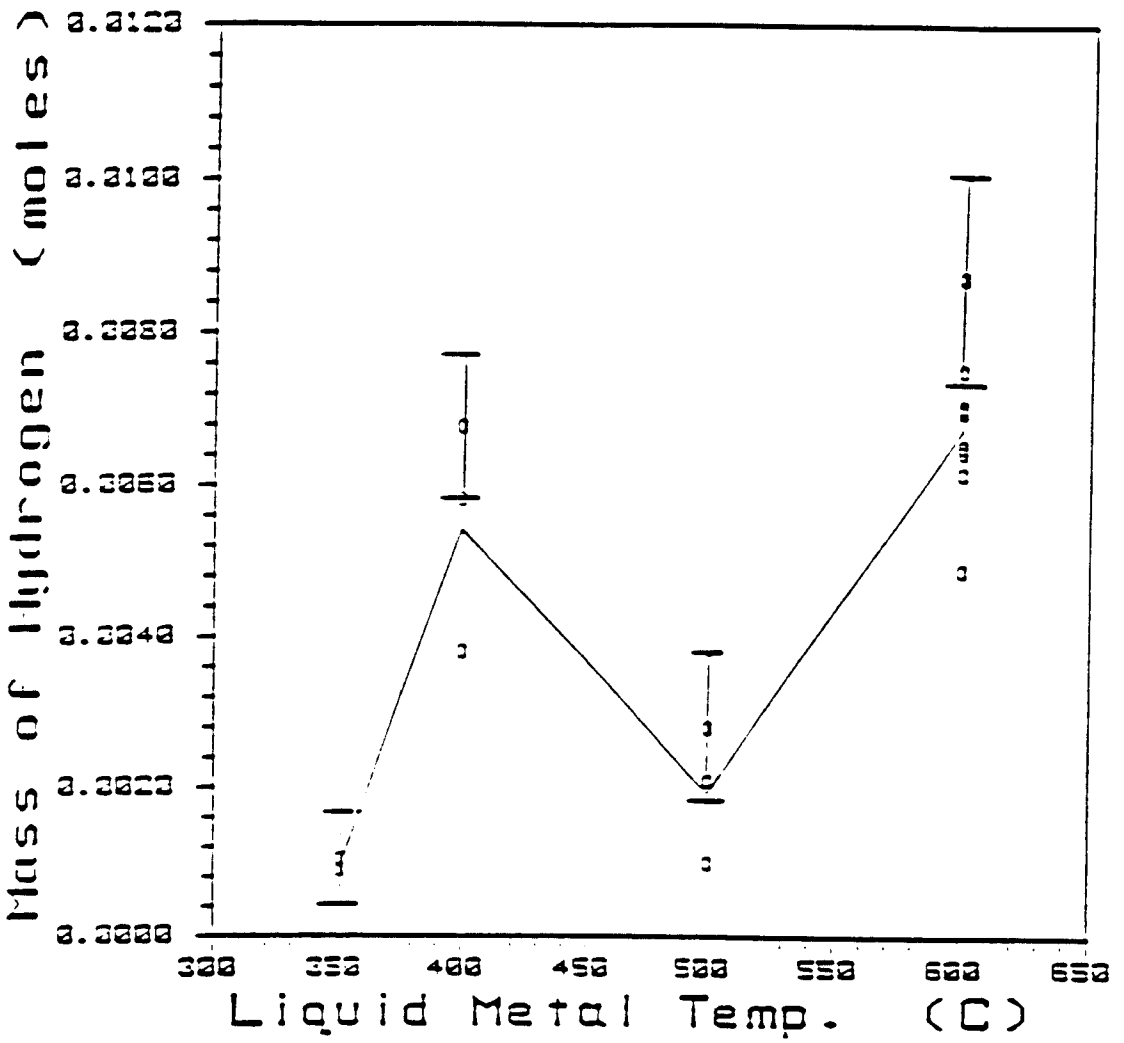

Figure 3.2: Mass of H_2 at 200sec as a function of the initial liquid metal temperature (Herzog, [6]).

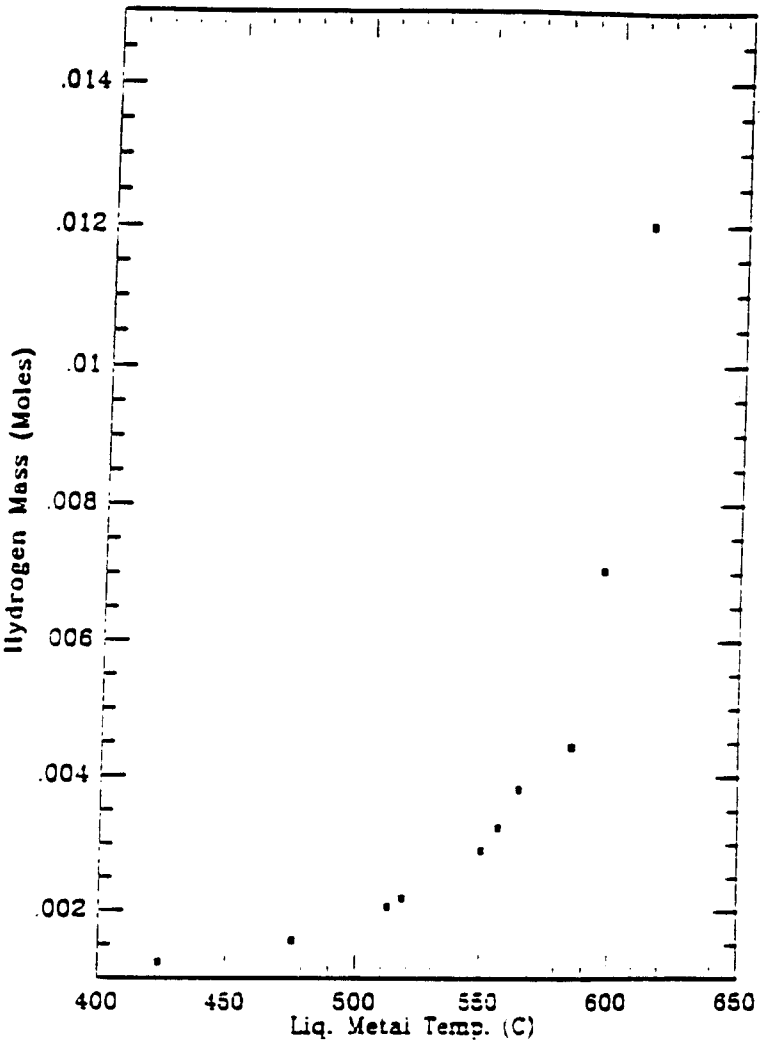

Figure 3.3: Mass of H_2 at 200sec as a function of liquid metal temperature (Lomperski [16]).

Material	Melt Temperature	Injection Pressure	Subcooling
Pb	500°C	1, 5, 10, 20. 25 bar	75°C, 43°C, 10°C
$Li_{17}Pb_{83}$	500°C	"	"
Li_7Pb_2	800°C	"	"
Li	500°C	"	"

Table 3.2: The test matrix of Kranert and Kottowski[12, p.10]

Kranert and Kottowski [12] [2] were interested in the combined thermal and chemical fuel/coolant interactions. In order to evaluate qualitatively the difference in the thermohydraulic behavior of different Li based fuels (eutectic $Li_{17}Pb_{83}$, Li_7Pb_2, Li, and Pb) when mixed with H_2O, they have performed a series of small-scale experiments at various injection pressures[3], p_{inj}, fuel and coolant temperatures.

The experimental apparatus (it was the same one used by Kottowski and Grossi[11]) and its measuring points are shown in fig. 3.4. The apparatus has a 2m long, 9mm I.D. driver section separated from the 24mm I.D., 170mm long austenitic steel reaction tube by a three-way ball valve. The 22mm I.D. (wall thickness is 0.8mm) capsule contains the fuel. Filling height of all fuels but lithium was 50mm (6.3mm of Li). The test matrix of the performed experiments is given in table 3.2.

During the experimental runs the following parameters were measured:

- pressures p_1 and p_2 (fig. 3.4) right above the three-way valve,
- fuel temperature T_m, and
- coolant temperature T_c.

[2]This work will be referred to in this proposal as Kranert.

[3]Injection pressure, p_{inj}, was defined as the "initial pressure difference between the reaction tube and the water in the expansion system.[12. p.1]"

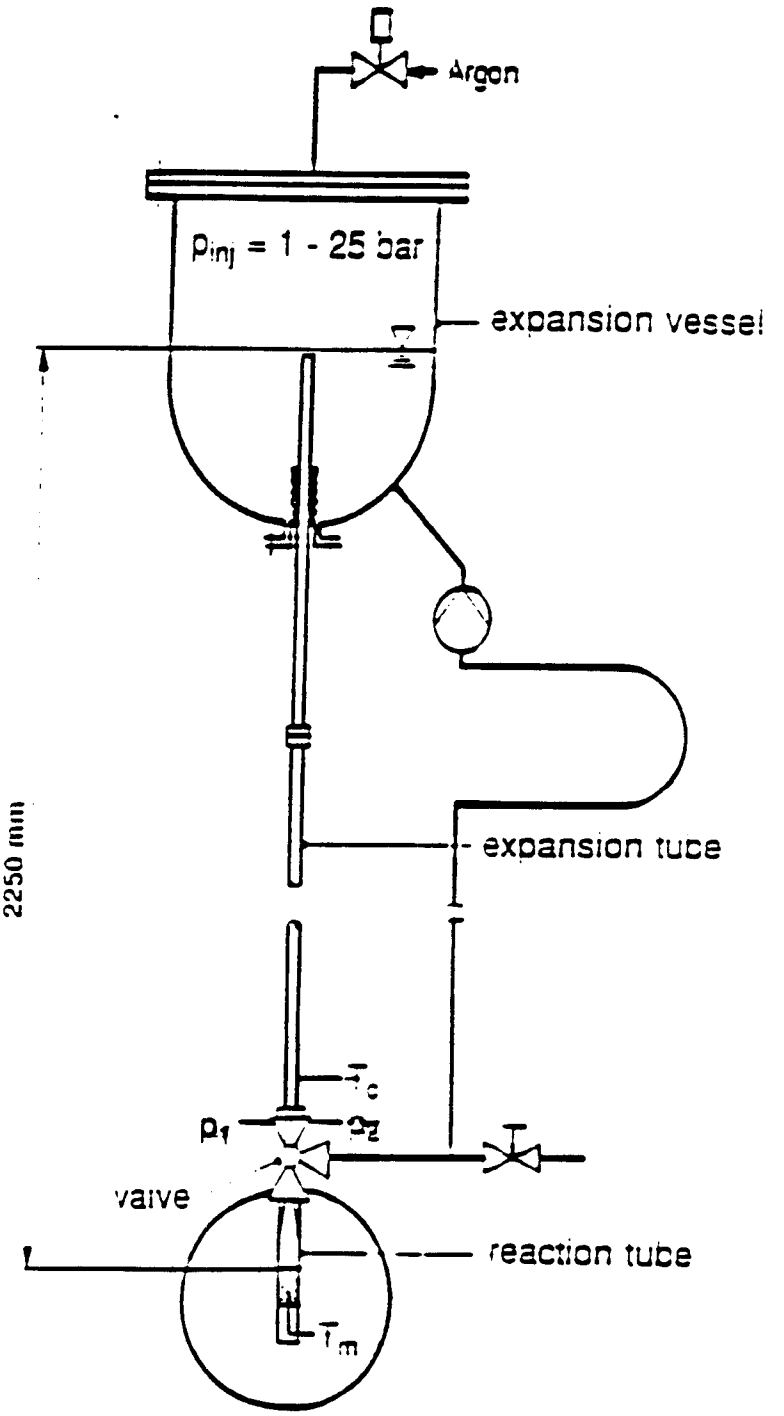

Figure 3.4: Experimental apparatus of Kranert and Kottowski and its measuring points [12, p.11]

Pressure and temperature evolution for Pb, Li, Li_7Pb_2, and $Li_{17}Pb_{83}$ are given in figures 3.5 and 3.6 for subcooling temperature of 75°C and injection pressures of 1bar and 20bar, respectively.

The experiments have shown that the chemical reaction becomes more dominant as the concentration of Li in fuel increases. In case of $Li_{17}Pb_{83}$ a violent thermal reaction is inhibited due to the attenuating effect of H_2 produced. The chemical reaction intensifies the reaction only at high driving pressures and high coolant temperatures. But in case of Li_7Pb_2 as well as of Li, the interaction seems to be governed by the chemical reaction under all conditions. In pure Li experiments a thermal fuel/coolant interaction was suppressed to the greatest extent.

Kranert's experiment was well designed and as such it allowed him to perform a large number of good experiments. The major shortcoming of his design is the difference in diameter between the reaction tube and the driver section. They should have been of the same diameter to assure one-dimensional behavior. Also, the data analysis would have been more accurate and complete if he had installed more dynamic pressure transducers along the shock tube and in the reaction chamber, and if he was able to monitor the change in hydrogen concentration in time.

Kranert's design has directly influenced the design of our shock tube. The experimental data that he has collected has helped us to set the design operating limits.

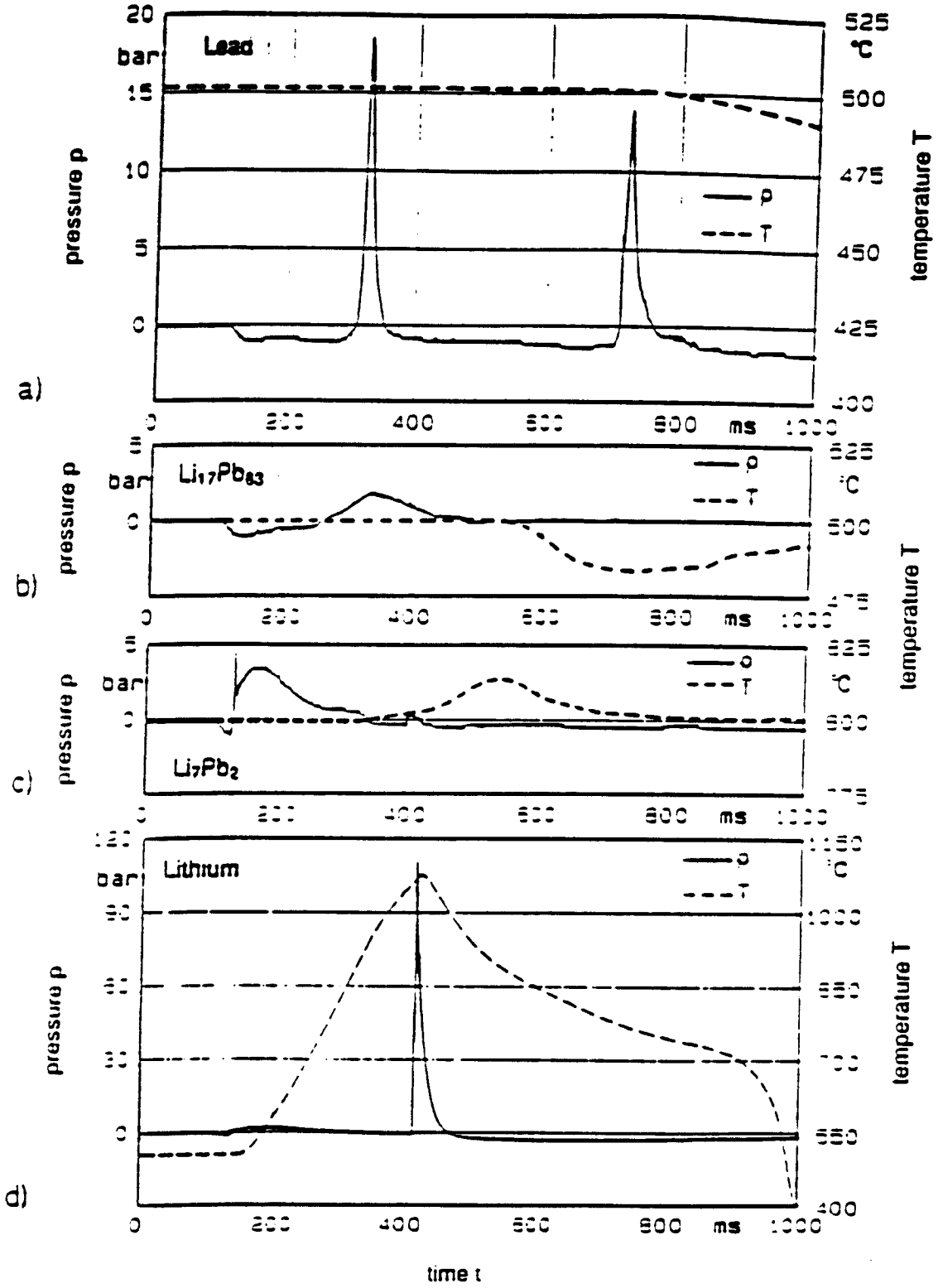

Figure 3.5: Pressure and temperature evolution of Pb, $Li_{17}Pb_{83}$, Li_7Pb_2, and Li as a function of time for p_{inj}=1bar [12].

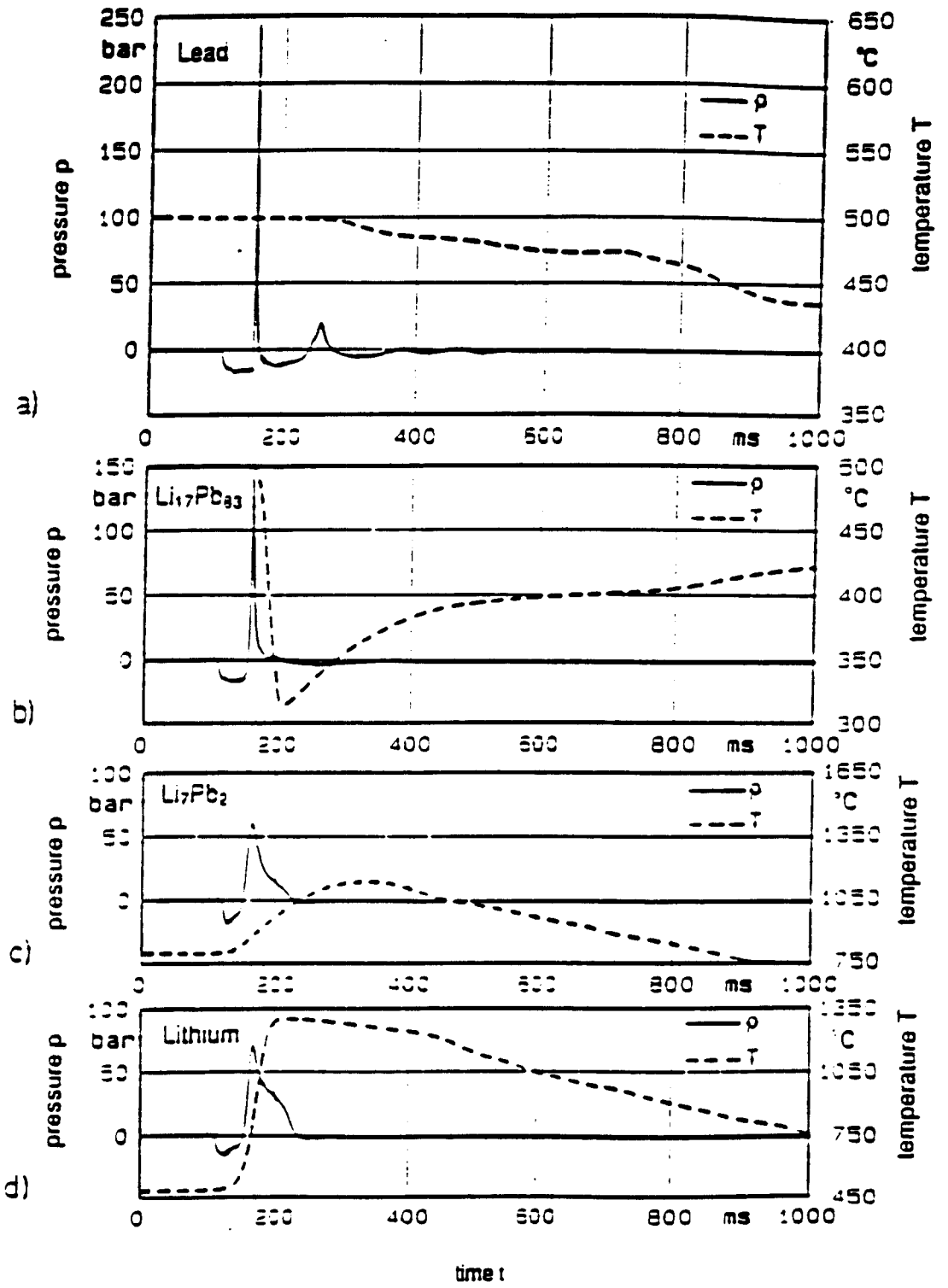

Figure 3.6: Pressure and temperature evolution of Pb, $Li_{17}Pb_{83}$, Li_7Pb_2, and Li as a function of time for p_{inj}=20bar [12].

3.2.2 Physical Models

Herzog's model [6]

In order to analyze his experimental data (given in the section 3.2.1), Herzog has developed two models: the kinetic reaction rate (KRR) model and liquid metal transport reaction (LMTR) model, which predict hydrogen production rate. The models are based on the following assumptions:

1. the reaction occurs only on the interaction surface,
2. the problem is one-dimensional, where the z-axis is perpendicular to the interaction surface,
3. thermodynamic properties are constant,
4. there is no convective motion in either the gas or liquid metal,
5. the gas phase is behaving as an ideal gas,
6. the concentrations (of both, the fuel and the coolant) and the liquid metal temperature only vary axially,
7. the lead concentration does not vary throughout the $Li_{17}Pb_{83}$ pool, and
8. the liquid metal volume change due to the reaction is negligible; the liquid metal is incompressible.

In figure 3.7 the reference coordinate system for both models is shown. The bottom of the liquid metal pool coincides with the origin of the coordinate system. Therefore, the liquid metal layer thickness equals s and the gas layer thickness is equal to $g - s$.

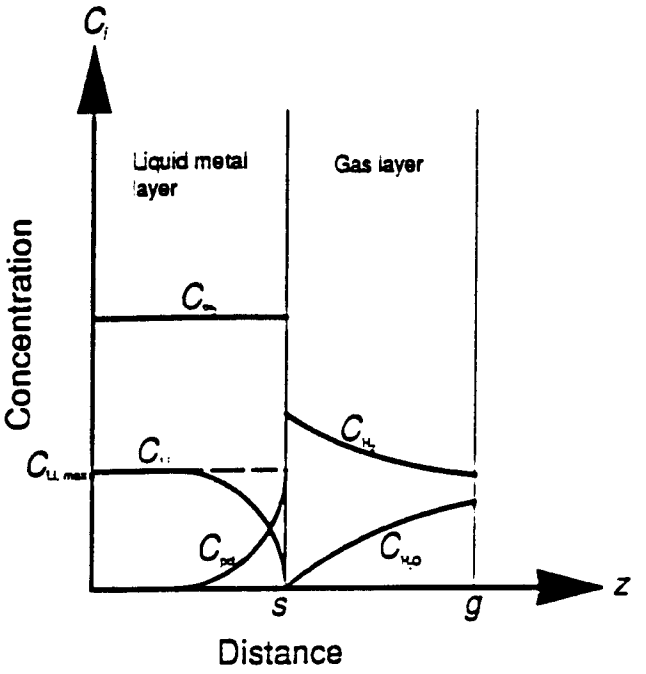

Figure 3.7: Reference coordinates for KRR and LMTR models [6].

According to the kinetic reaction rate model, the rate of diffusion of the reactants (Li and water vapor) towards and products (LiOH or Li_2O, and H_2) away from the interaction surface is greater than the rate at which the reactants at the surface mix and react. Therefore, this model states that the course of the reaction is controlled by the kinetic rate of the reaction which is defined in the following equation [6, p.115]:

$$R_{\mathrm{Li}} = \frac{a_{\mathrm{H_2O}}}{a_{\mathrm{Li}}} R_{\mathrm{H_2O}} = k C_{\mathrm{H_2O}}{}^{\mathrm{n}} C_{\mathrm{Li}}{}^{\mathrm{m}} \tag{3.1}$$

where R_{Li} and $R_{\mathrm{H_2O}}$ are the rates at which Li and H_2O are consumed by the reaction, a_{Li} and $a_{\mathrm{H_2O}}$ are the Li and H_2O stoichiometric coefficients, k is a reaction rate coefficient, m and n are the Li and H_2O concentration reaction exponents, and C_{Li} and $C_{\mathrm{H_2O}}$ are Li and H_2O molar concentrations.

It is assumed that the reaction rate coefficient temperature dependence is of the Arrhenius form:

$$k(T) = k_0 \exp\left(-\frac{\Delta E_\mathrm{k}}{RT}\right) \tag{3.2}$$

where k_0 is the reaction rate coefficient proportionality constant, ΔE_k is the reaction rate coefficient activation energy, R is the universal gas constant, and T is the absolute temperature.

On the other hand, the LMTR model (which is "essentially a simplification of the more general KRR model" [6, p.117]) says that the diffusion rate of the reactants and products controls the reaction, as given by the expression

$$R_\mathrm{Li} = -D_\mathrm{lm}\frac{\partial C_\mathrm{Li}}{\partial z} \tag{3.3}$$

where D_lm is the liquid metal layer diffusion coefficient.

Again, the liquid metal diffusion coefficient is assumed to have the Arrhenius form:

$$D_\mathrm{lm} = D_0 \exp\left(-\frac{\Delta E_\mathrm{d}}{RT}\right) \tag{3.4}$$

where D_0 is the diffusion coefficient proportionality constant and ΔE_d is the diffusion coefficient activation energy.

The basic equations solved in both models were the equation of continuity and the equation of energy conservation. In general, the equation of continuity for each species of a multicomponent system is given by, [6, p.119]

$$\frac{\partial C_i}{\partial t} = -\frac{\partial}{\partial z}(C_i v + \dot{J}_i) \tag{3.5}$$

where t is time, v is the mass average velocity, and $\dot{J}_i$ is the molar flowrate of species i.

The boundary conditions are: at $z = 0$, $\frac{\partial C_{\mathrm{Li}}}{\partial z} = 0$, and at $z = s$, $C_{\mathrm{Li}} = 0$. The initial condition is given by $C_{\mathrm{Li}}(z,0) = C_{\mathrm{Limax}}$ where $C_{\mathrm{Limax}} = C_{\mathrm{pd}}(z,t) + C_{\mathrm{Li}}(z,t)$ is the molar concentration of lithium in pure $Li_{17}Pb_{83}$, and $C_{\mathrm{pd}}(z,t)$ is the molar concentration of liquid metal products.

The velocity term in equation 3.5 is ignored by assumption 4 so that we get

$$\frac{\partial C_i}{\partial t} = -\frac{\partial \dot{J}_i}{\partial z} \tag{3.6}$$

Under the assumptions 4 and 8, the energy equation of the liquid metal layer can be expressed as [6]:

$$\rho \frac{DH}{Dt} = -\frac{\partial}{\partial z}\left(-k_{\mathrm{lm}}\frac{\partial T}{\partial z} + \sum_i M_i H_i \dot{J}_i\right) + \frac{Dp}{Dt} \tag{3.7}$$

where ρ is the density, H is the enthalpy, k_{lm} is the liquid metal thermal conductivity, and M_i is the molecular weight of species i.

Assuming constant properties we get the following equation:

$$\rho c_{\mathrm{p}} \frac{\partial T}{\partial t} = k_{\mathrm{lm}}\frac{\partial^2 T}{\partial z^2} - \sum_i \left(\dot{J}_i M_i c_{\mathrm{p}_i}\frac{\partial T}{\partial z} + M_i H_i \frac{\partial \dot{J}_i}{\partial z}\right) \tag{3.8}$$

where c_{p_i} is the specific heat of species i.

The initial condition for the energy equation is $T(z,0) = T_{\mathrm{tc}}(0)$ where T_{tc} is a known temperature at the base of the metal pool. The boundary conditions are: at $z = 0$, $T(0,t) = T_{\mathrm{tc}}(t)$ and at $z = s$, $q_{\mathrm{conv}} = q_{\mathrm{cond}} + q_{\mathrm{gen}}$, where q_{conv} is the heat transfer by convection from the reaction surface to the vapor film, q_{cond} is the heat transfer by conduction from the base to the interaction surface, and q_{gen} is the heat generated at the interaction surface as a result of the exothermic reaction.

Before the models can be used the following parameters must be specified:

KRR model: "the liquid metal diffusion coefficient, the water vapor boundary value at the edge of the gas and vapor film, the reaction rate exponents m and n, and the reaction rate coefficient parameters (ΔE_k and k_0)"[6, p.131], and

LMTR model: the liquid metal diffusion coefficient parameters (ΔE_d and D_0).

For both models, the values of ΔE_k and k_0 (in the KRR model) and ΔE_d and D_0 (in the LMTR model) were varied until the total mass of hydrogen produced during the first 200sec matched the experimentally obtained values.

The experimental data measured during the first few seconds were used to estimate the initial H_2 generation rate required by the models.

It was found that the KRR model would work only with values of the liquid metal diffusion coefficient greater than $10^{-7}m^2/s$. In the case of the LMTR model, the derived liquid metal diffusion coefficient and the theoretical $Li_{17}Pb_{83}$ diffusion coefficient agreed well for all the tests done with liquid metal initial temperature of 600°C. The overall conclusion is that the LMTR model describes the $Li_{17}Pb_{83}/H_2O$ reaction more accurately than the KRR model [6, p.139], and therefore it proves that the $Li_{17}Pb_{83}/H_2O$ reaction is controlled by the rate of diffusion in liquid metal. In addition to that, it was shown that the reaction rate strongly depends on the liquid metal temperature.

Biney's model[1,16], (modified Herzog's model)

The one-dimensional liquid metal transport model for the small-scale $Li_{17}Pb_{83}/H_2O$ reaction proposed by Herzog [6] was improved by Biney [1]. In order to give an estimate of the chemical reaction rate and to find the relationship between the

reaction rate coefficient and the initial liquid metal temperature, this improved version was applied on data measured by Lomperski [16] (fig. 3.3).

Biney used the same set of equations as Herzog (3.5, 3.8) with the same initial and boundary conditions, and he accepted the same assumptions.

In order to get better agreement between the model's estimate of hydrogen production during the reaction and the experimental results, Biney has modified Herzog's original model in the following way:

- stable film boiling condition was checked for in the model and Collier's expression for the stable film boiling heat transfer coefficient (obtained from the theory of film boiling on a flat horizontal surface) [1, p.2] have been included in the model,

- all vapor properties were made temperature dependent and were calculated for the mean temperature.

The model's predictions of hydrogen production and hydrogen production rate per unit area are given in figures 3.8 and 3.9. It can be seen that in the beginning (i.e. up to $\sim$ 10sec) of the chemical reaction its rate decreases rapidly, but for reaction times greater than $\sim$10s the reaction rate decreases linearly. The initial hydrogen production rate time dependence was found to be of parabolic form [16]:

$$\frac{\partial}{\partial t}\left(\frac{m_{H_2}}{A}\right)^2 = D_{H_2} \exp\left(-\frac{\Delta E_{H_2}}{RT}\right) \tag{3.9}$$

where m_{H_2} is the mass of hydrogen, A is the interaction area, D_{H_2} is the hydrogen production rate proportionality constant, and ΔE_{H_2} is the hydrogen production rate activation energy. For later reaction times, the chemical

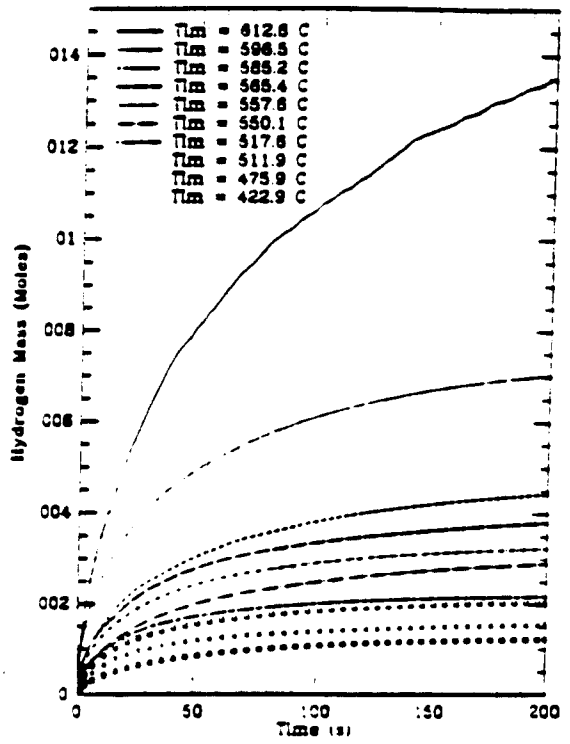

Figure 3.8: Time history of hydrogen production (Biney's model [1]).

reaction rate can be represented by a linear rate law [1]:

$$\frac{1}{A}\frac{\partial N_{H_2}}{\partial t} = D_{H_2}\exp\left(-\frac{\Delta E_{H_2}}{RT}\right) = D_{lm}C_{Limax} \tag{3.10}$$

where N_{H_2} is the number of moles of hydrogen. The mean values of D_{H_2} and ΔE_{H_2} obtained from the model are: $D_{H_2} = 1.52\times10^{6}\text{g}^2/(\text{cm}^4\text{sec})$ and $\Delta E_{H_2} = 89.0\times10^{6}\text{J/mole}$ at the beginning of the reaction, and $D_{H_2} = 6.6\times10^{6}\text{moles}/(\text{m}^2\text{sec})$ and $\Delta E_{H_2} = 1.233\times10^{5}\text{J/mole}$ at later times of the reaction. Also, it was found that the reaction constants ΔE_d, ΔE_{H_2}, and D_{H_2} are not functions of the initial liquid metal temperature, while the constant D_0 is.

If we are discussing the applicability of Biney's model to our shock-tube experiments then the major shortcoming of the model should be mentioned

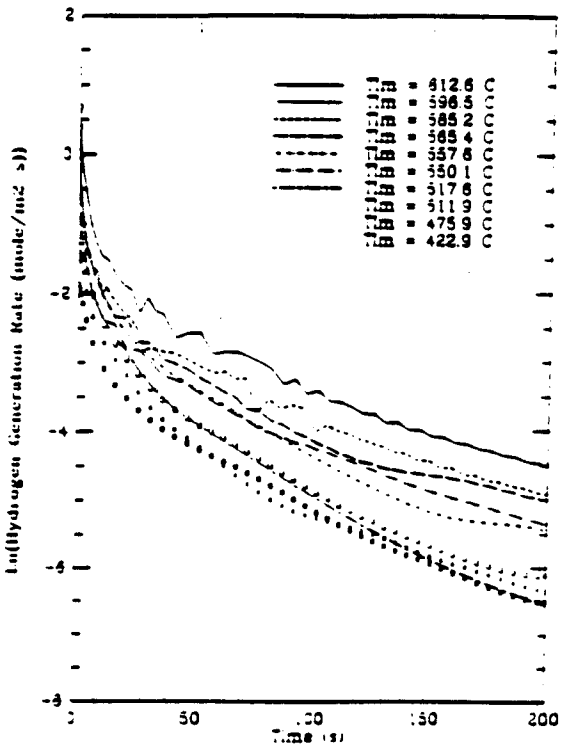

Figure 3.9: Time history of hydrogen production rate (Biney's model [1]).

first. That is the assumption of the well defined interaction surface, undisturbed during the experiment; i.e., any kind of the surface disturbance has been neglected. In our experiments with system pressures larger than 1bar (as used in Herzog's and Lomperski's experiments) we expect to have fuel fragmentation and mixing with coolant to some extent (the higher the system pressure the better the mixing). Therefore, Biney's model can not be directly used for data analysis in those cases. But, his model could be used for the analysis of data which will be obtained in experimental runs identical (i.e. with the acceptable scaling factor) to those done by Herzog and Lomperski.

Kranert's model [12]

In order to evaluate his experimental data Kranert has used a macroscopic model for a shock-tube [12]. He has approximated the water column by a slug and has assumed that:

- water column velocity is zero after hitting the liquid metal surface,
- pressure and velocities perpendicular to the liquid metal surface are equal (boundary conditions),

The kinetic energy of the water hitting the liquid metal, E_{kin_C}, is given by the expression:

$$E_{kin_C} = E_{abs} + E_r = m_C \frac{{v_C}^2}{2} \tag{3.11}$$

where E_{abs} is the absorbed energy, E_r is the reflected energy, m_C is the mass of the water column, and v_C is the water column impact velocity.

The velocity v_C can be calculated from the expression for the increase in pressure at impact, Δp, which is proportional to the water density, ρ_C, sound velocity in the water c_C, and the velocity difference, Δv_C, (with the assumption of zero water column velocity after impact, the velocity difference is equal to the impact velocity v_C). Now E_{kin_C} can be expressed as:

$$E_{kin_C} = \frac{m_C}{2} \left(\frac{\Delta p}{c_C \rho_C} \right)^2 \tag{3.12}$$

The absorbed energy is used for the fragmentation and mixing. Introducing the reflection coefficient [12]:

$$R \equiv \frac{E_r}{E_{kin_C}} = \left(\frac{\rho_f c_f - \rho_C c_C}{\rho_f c_f + \rho_C c_C} \right)^2 \tag{3.13}$$

(ρ_f and c_f are the fuel density and sound velocity in fuel), the equation for E_{abs} becomes:

$$E_{abs} = 4\frac{\rho_f c_f \rho_c c_c}{(\rho_f c_f + \rho_c c_c)^2} E_{kin_c} \tag{3.14}$$

In order to evaluate the mechanical energy released from the fuel/coolant interaction, Kranert started from the rising water column energy balance equation:

$$dU_c + dE_{pot_c} + dE_{kin_c} = \sum \delta Q_c + \sum \delta W_c \tag{3.15}$$

where U_c, E_{pot_c}, and E_{kin_c} are the internal, potential, and kinetic energy of the water column, Q_c is the heat transferred to the water column, and W_c is the work done by the water column.

Neglecting dU_c, dE_{pot_c}, and δQ_c, the mechanical work release gets the form

$$\delta W_c = \frac{1}{2} m_c v_c^2(t) \tag{3.16}$$

Kranert defines the driving pressure by

$$p_{dr}(t) = p_{1,2}(t) - p_{inj} \tag{3.17}$$

The integration of the Bernoulli equation for the water column results in

$$\rho_c l_c v_c(t) = \int_t^{t+dt} p_{dr}(t) dt \tag{3.18}$$

where l_c is the water column length. Finally, equations 3.16 and 3.18 give the expression for the mechanical energy release of the fuel/coolant interaction:

$$\delta W_c = \frac{1}{2} \frac{m_c}{\rho_c{}^2 l_c{}^2} \left(\int_t^{t+dt} p_{dr}(t) dt \right)^2 \tag{3.19}$$

Applying this model to the experimental data obtained from the $Li_{17}Pb_{83}/H_2O$ interactions (section 3.2), Kranert calculated (among other things): a) fragmented melt mass vs. absorbed energy (figure 3.10 on page 52), b) specific

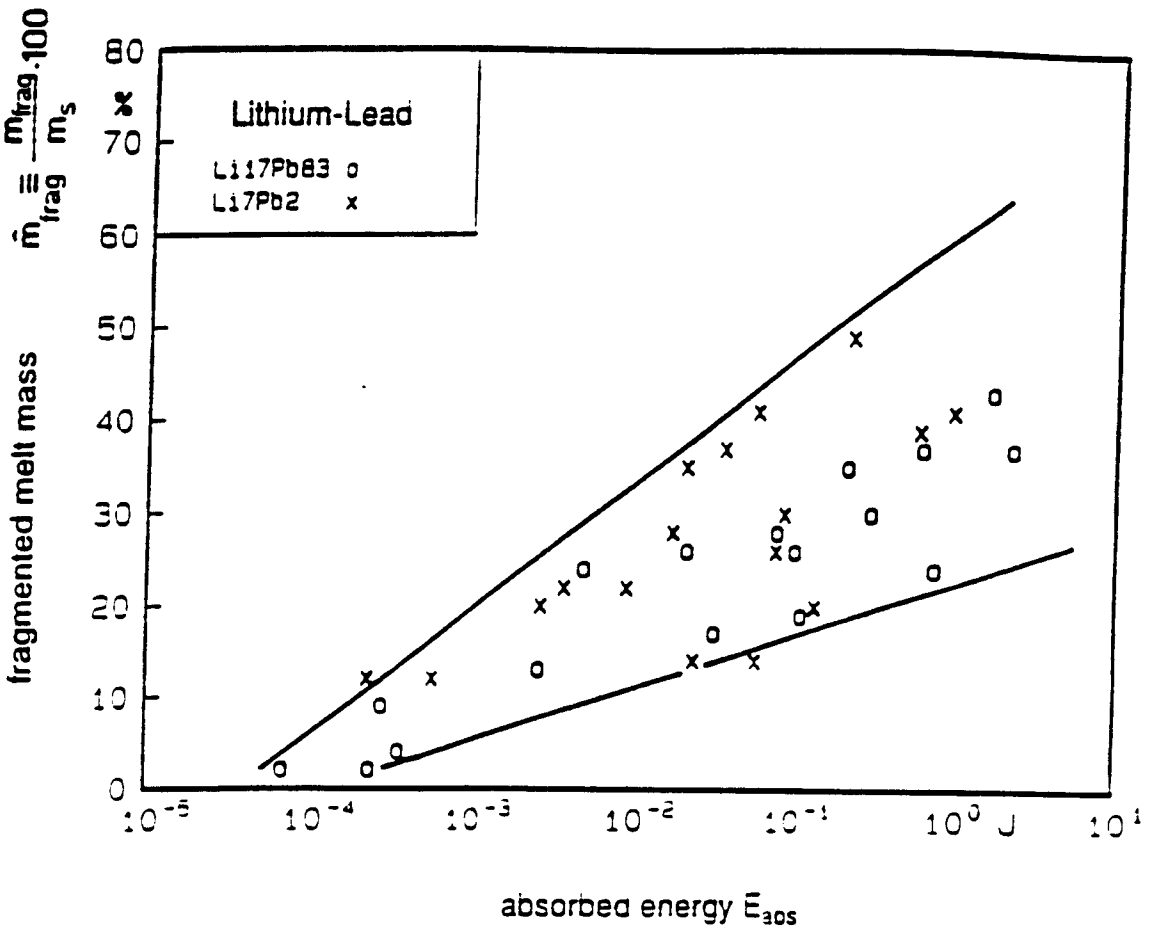

Figure 3.10:
Fragmented melt mass as a function of the absorbed energy (m_{frag} is the fragmented liquid metal mass and m_s is the initial liquid metal mass).[12, p.15]

absorbed energy vs. injection pressure for three coolant temperatures, (figure 3.11 on page 53), and c) specific mechanical energy vs. specific absorbed energy for three coolant temperatures, (figure 3.12 on page 54)[12]. The graphs show that the absorbed energy per unit mass increases with increasing injection pressure and that the fragmented melt mass increases with the absorbed energy. As expected, higher values of released specific mechanical work correspond to higher values of the specific absorbed energy.

Let us consider some limitations in Kranert's model:

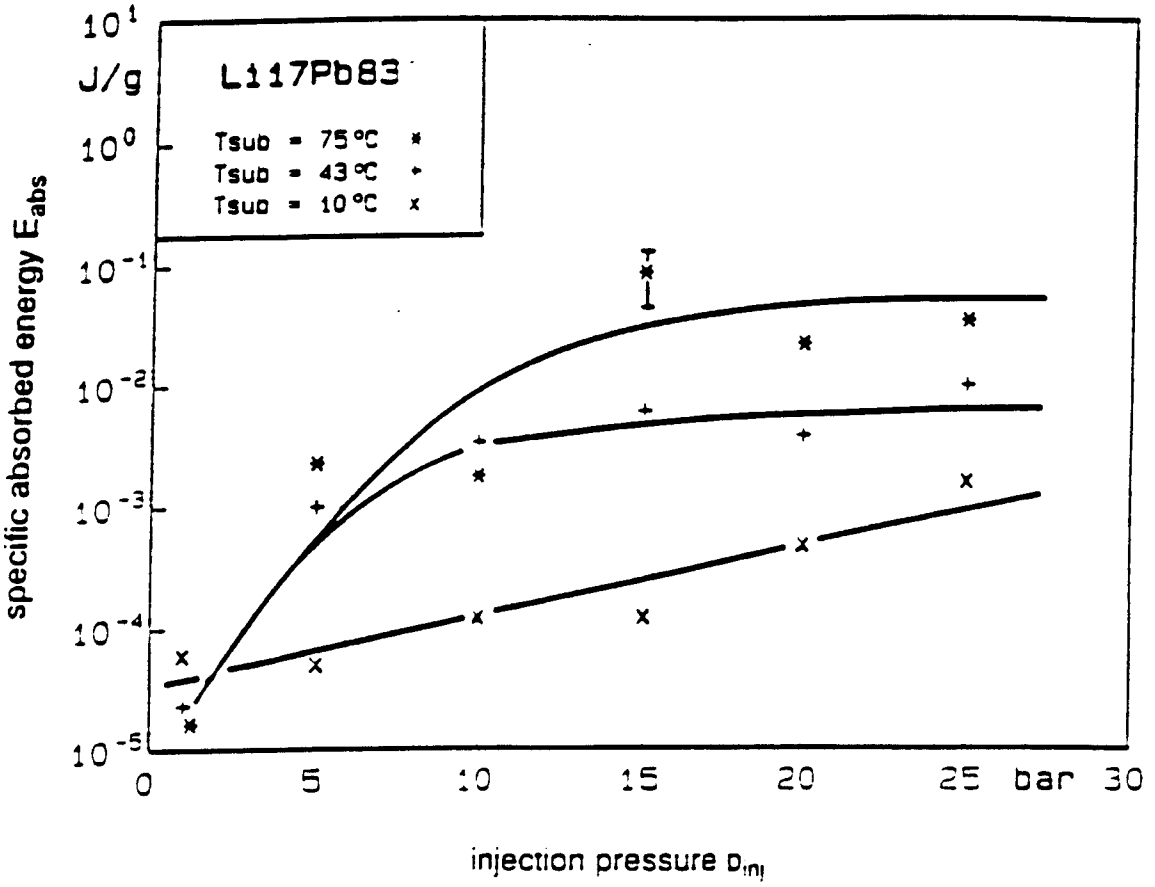

Figure 3.11: Specific absorbed energy as a function of the injection pressure [12, p.17].

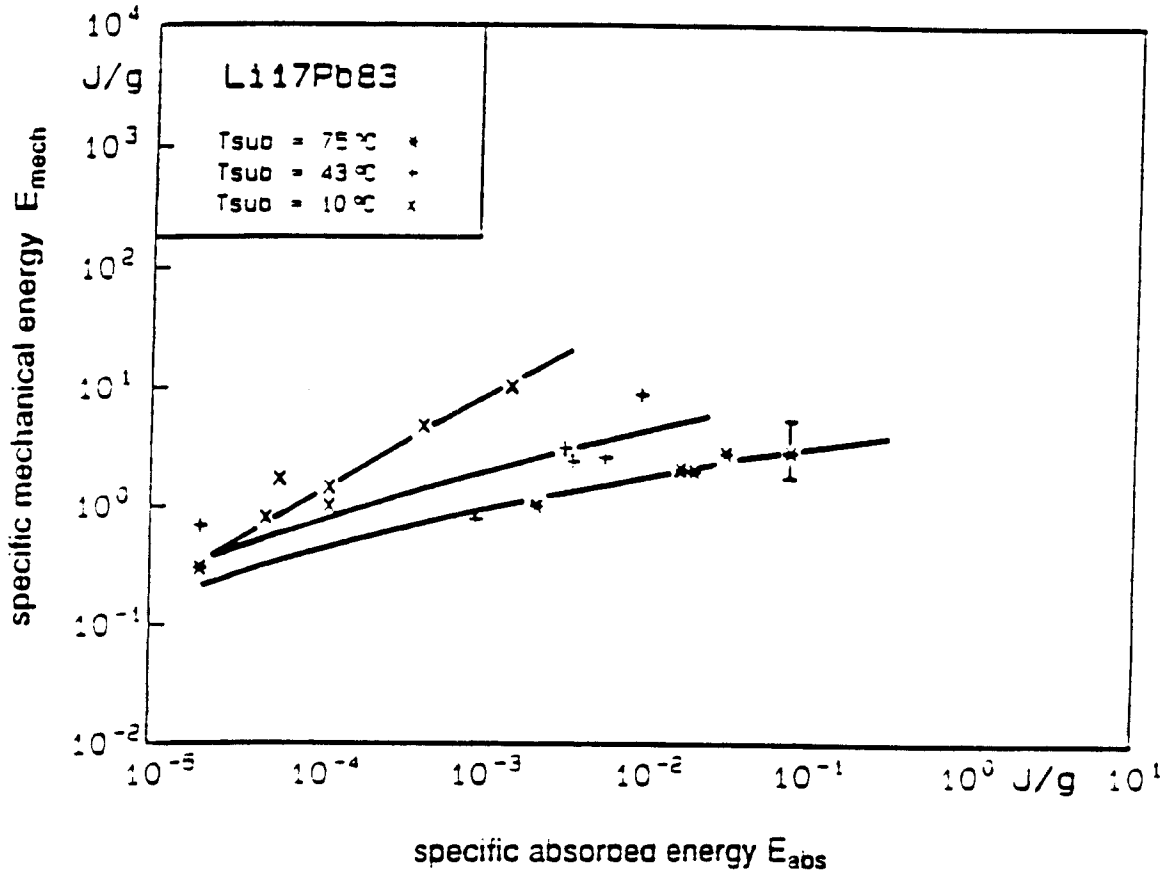

Figure 3.12: Specific mechanical energy as a function of the specific absorbed energy [12. p.20].

- In Kranert's model, the water column impact velocity is defined through the expression for the increase in pressure at impact (equations (3.11) and (3.12))

$$\Delta p = \rho_C c_C \Delta v_C \tag{3.20}$$

This equation is valid only if there is a complete vacuum in the region above the liquid metal. In reality, the pressure after impact is smaller than the theoretical water-hammer pressure [22].

- Equation (3.16) is only approximate since its right-hand side represents the instantaneous value of the kinetic energy instead of the change in kinetic energy with time.

- The way he defines the driving pressure (eq. (3.17)) is again approximate since p_{inj}, according to its definition in section 3.2.1, does not vary in time. Instead of p_{inj}, the variable expansion vessel pressure should be used. That requires the installation of a pressure transducer in the expansion vessel (fig. 3.4).

- Instead of the pressure $p_{1,2}(t)$, the variable pressure in the reaction chamber should be used in eq. (3.17). That also requires the installation of a pressure transducer in the reaction chamber.

- Even if he was interested in the $Li_{17}Pb_{83}/H_2O$ chemical reaction, Kranert did not go beyond a schematic presentation of the lithium concentration evolution during the reaction. The reason for that probably lies in the fact that Kranert was the first one to try to do a more detailed quantitative analysis of $Li_{17}Pb_{83}/H_2O$ interaction in a shock-tube geometry.

Chapter 4

Proposed Research

This chapter presents the proposed research. The research goals and the experimental apparatus are presented. This also includes a short description of the shock-tube auxiliary equipment, measurement system and the data acquisition system. Finally, the experimental procedure is presented together with the proposed test matrix.

4.1 Research Goals

The overall goal of this research is to investigate the explosive characteristics and the chemical reactivity of liquid metal (in particular lithium-lead) in a controlled one-dimensional apparatus and examine if the results can be predicted by the simple correlation model of Herzog [6], improved by Biney at al[1]. Therefore, to improve upon past experiments, these detailed shock-tube experiments must be designed to include:

- pressure and temperature measurements and H_2 samples collection during the experiment.
- H_2 concentration measurements,

- chemical analysis of the debris, and
- particle size distribution characterization of the debris (if possible).

The experimental data will be compared with:

- JRC Ispra's data [12], obtained on an apparatus of the same scale, and
- Herzog's [6] and Lomperski's [16] data (obtained on apparatus of much smaller scale), if possible.

So far there is no available physical model that could be directly used for our data analysis. In section 3.2.2 available models were presented. On one hand, there is Kranert's macroscopic model for a shock-tube which does not deal with the chemical effects of the $Li_{17}Pb_{83}/H_2O$ reaction. On the other hand, Herzog's and Biney's models give us only the estimate of the hydrogen production rate with time given a known exposed surface area. None of these models include mixing and fragmentation[1] upon impact.

What is needed for our data analysis is a physical model that would initially incorporate the existing macroscopic shock-tube model and macroscopic reaction rate model. Eventually, the model should incorporate the effects of mixing and fragmentation in the early stage of $Li_{17}Pb_{83}/H_2O$ interaction.

Therefore, in the final stage of this project the existing models (that cover some aspects of the process in a shock-tube) should be combined, and the resulting model should be used for the analysis of the obtained data.

[1] Mechanisms of mixing and fragmentation are described and modelled in vapor explosion literature (e.g. [18,19]).

4.2 Experimental Apparatus

The main components of the experimental set-up are given in figure 4.1 (p. 59). The coolant (in the compression tube (3)) is separated from the fuel (in a reaction tube (6)) by a scored metal rupture disc. Since the fuel/coolant contact can produce disruptive mechanical forces, the shock-tube is clamped to the vertical I-beam which is firmly mounted to the concrete laboratory floor and a wall column. In the case of the shock-tube clamps failure, the impulse kinetic energy will be absorbed by the Enidine shock-absorber (8) mounted below the shock-tube. A HAAKE constant temperature circulator (10) (operating temperature range from -30 °C up to 100 °C) is used to control the coolant temperature and to set the coolant level. The oven (7) temperature is controlled by an Omega temperature controller. Temperature of the cover gas in the reaction chamber can be adjusted by circulating argon through that region or by changing the water temperature and flowrate through the heat exchanger (5). A second HAAKE constant temperature bath (10) is used as a water (that goes through the heat exchanger) reservoir and circulator. In order to be able to change the pressure (i.e. vacuum) in the gas region of the reaction chamber, a Welch DuoSeal vacuum pump (11) is installed.

In the preparation phase of the experiment the upper portion of the apparatus (expansion vessel (2)) is filled with argon. Its pressure is set to such a value so that the difference of pressures, i.e. driving pressure, in the expansion vessel (system i.e. argon pressure) and reaction chamber is equal to the rupture disk burst value by operating (via the Keithley Data Acquisition

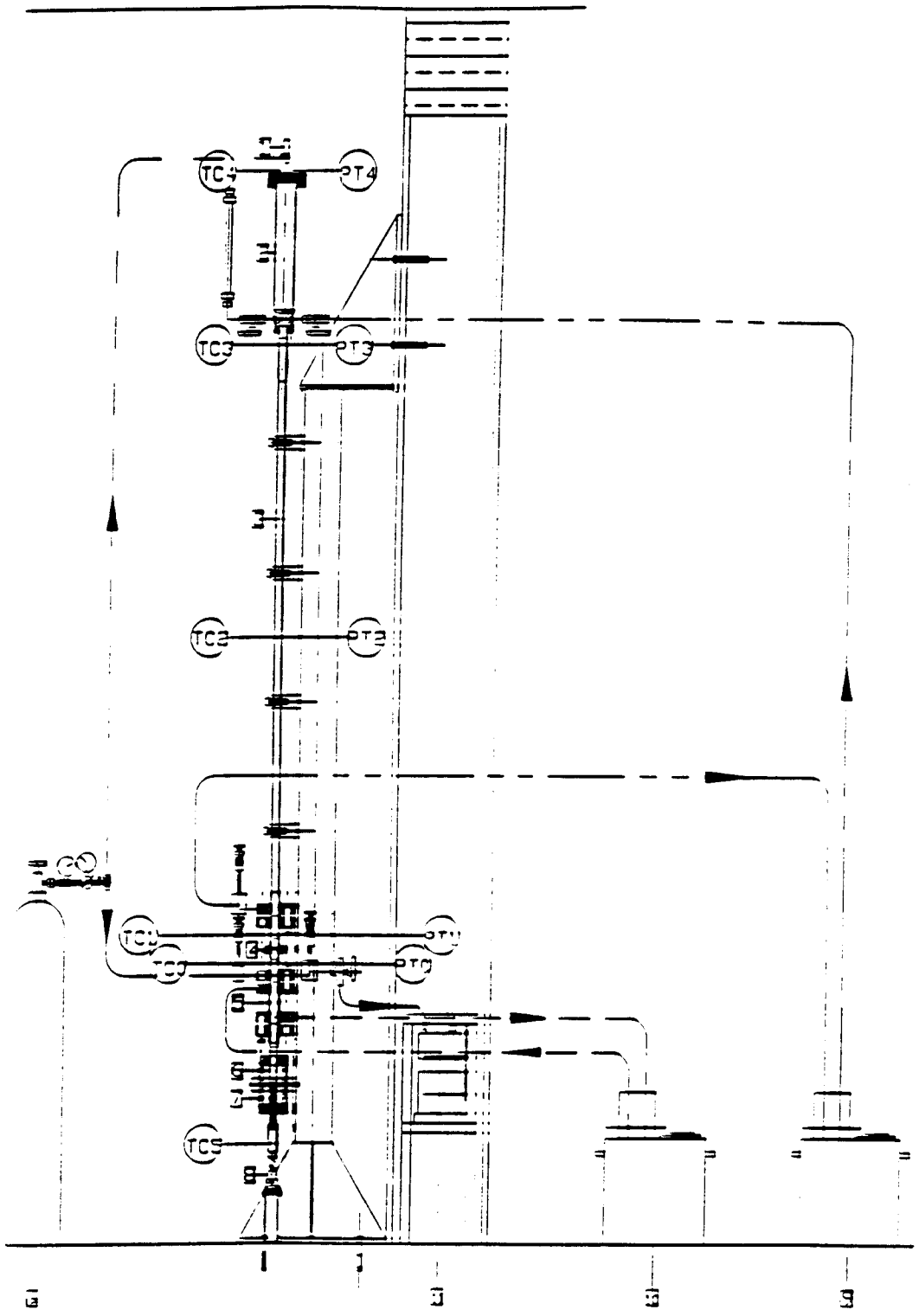

Figure 4.1: Shock-tube for the proposed research

System 500)[2] the ASCO 2-way piston type solenoid valve (1). In order to monitor the argon pressure during the preparation phase, a strain gauge pressure transducer is mounted on the top flange of the expansion vessel. Its output is fed through the preamplifier and DAS 500 and stored into an IBM-PC/XT (4.7MHz). Thermocouples (TC0-5), also connected to DAS 500, are used to measure fuel, coolant, and gas temperatures, while the readings are stored in the same personal computer. Dynamic pressure changes during the experiment are sensed by quartz pressure transducers (PT0-4). Amplified signals are temporarily stored in two LeCroy 8808A memories, and after the experiment is finished these are transferred into Club PC/AT compatible (12 MHz) computer.

In the following subsections the mechanical design, measurement and data acquisition systems are presented in greater detail.

4.2.1 Mechanical Design

On the basis of the previous similar small-scale shock-tube experiments [12] it was accepted to design[3] the shock-tube so that it can stand the maximum dynamic pressure of 250 bar and the maximum temperature in the reaction tube of 1500°C. The shock-tube consists of three stainless steel sections: the expansion vessel, the driver section (this includes the compression tube and all the other parts between the expansion vessel and the rupture disk), and the reaction chamber (this includes the reaction tube and all the other parts

[2]Referred to as DAS 500.

[3]Mechanical designing of the shock-tube was done by visiting engineer Mike Raz, with the help of Joe Krueger and the author. All the calculations and detailed drawings are given in [21].

	Inner diam. [mm]	Length [m]	Material
Expansion vessel	76.2	0.500	304 SS
Driver section	25.4	2.530	304 SS
Reaction chamber	24.0	0.584	321 SS
Fuel crucible[a]	22.0	0.118	321 SS

[a]The fuel crucible is placed inside the reaction tube.

Table 4.1: Dimensions of the shock-tube.

from the rupture disc to the bottom of the reaction tube). The dimensions and materials of the components are given in table 4.1.

The Fike Poly-SD rupture discs were chosen because they seemed to satisfy best our main requirements to open virtually instantaneously and without fragmentation and within the temperature and pressure limits of our experiments. They are scored (score lines define the bursting pattern) on the downstream (fuel) side. Depending on their thickness and composition (aluminum, nickel or inconel, in our case), discs rupture at a specified "stamped burst pressures"(within the standard manufacturing design range which depend on the stamped burst pressure).

4.2.2 Auxiliary Equipment

When dealing with $Li_{17}Pb_{83}$ or any other metal that oxidizes in open air, fuel preparation has to be done in a glove box. Therefore, the VAC HE-series Dri-Lab with an argon atmosphere, nearly free of moisture, oxygen and nitrogen, was purchased from the Vacuum/Atmospheres Company [24]. Its purification system recirculates the argon while removing water vapor and oxygen until the concentration is less than 5ppm by volume.

A model CN9111 Omega miniature microprocessor temperature controller is connected to a branch of specially designed electrical circuit through a solid state relay where the heater and its variable power supply are. An Omega vacuum formed ceramic fiber radiant heater (model CRFC-36/115-C, 76.2mm I.D., 228.6mm total length) was chosen, primarily because of its high power (700W at 120V), and good insulation (at maximum chamber temperature of 1100°C the outside surface temperature is ~180°C).

4.2.3 Measurement System

All the thermocouples are 1.587mm O.D. SS sheathed OMEGA quick disconnect miniature thermocouples. Thermocouples $T0, T1, T2, T3$, and $T4$ (figure 4.2) are of type E, and their tips are 9mm in the tube. Thermocouples $T5$ and $T6$ are of K type. $T5$ is used to measure the fuel temperature and it is placed (up to 20mm from its tip) in a ceramic protection tube. Its tip, protected by the 304 SS protection tube (the end of the tube that is in direct contact with fuel is closed, and the other end is welded to the bottom of the fuel crucible) is placed 20mm into the fuel crucible. $T6$ is placed between the heater and the reaction tube.

Two strain-gauge pressure transducers (one with 0-200psig, and the other one with 0-500psig pressure range), model 175A, Robinson-Halpern Co., are used to monitor the pressure in the expansion vessel during the preparation phase. When pressure is applied to the 17-4 PH SS diaphragm, the deflection is transmitted directly to the bonded foil strain gauge bridge. The output is 20mV±2% full scale, with infinite resolution.

Five miniature, quartz, charge mode PCB Piezotronics (Model 112A03)

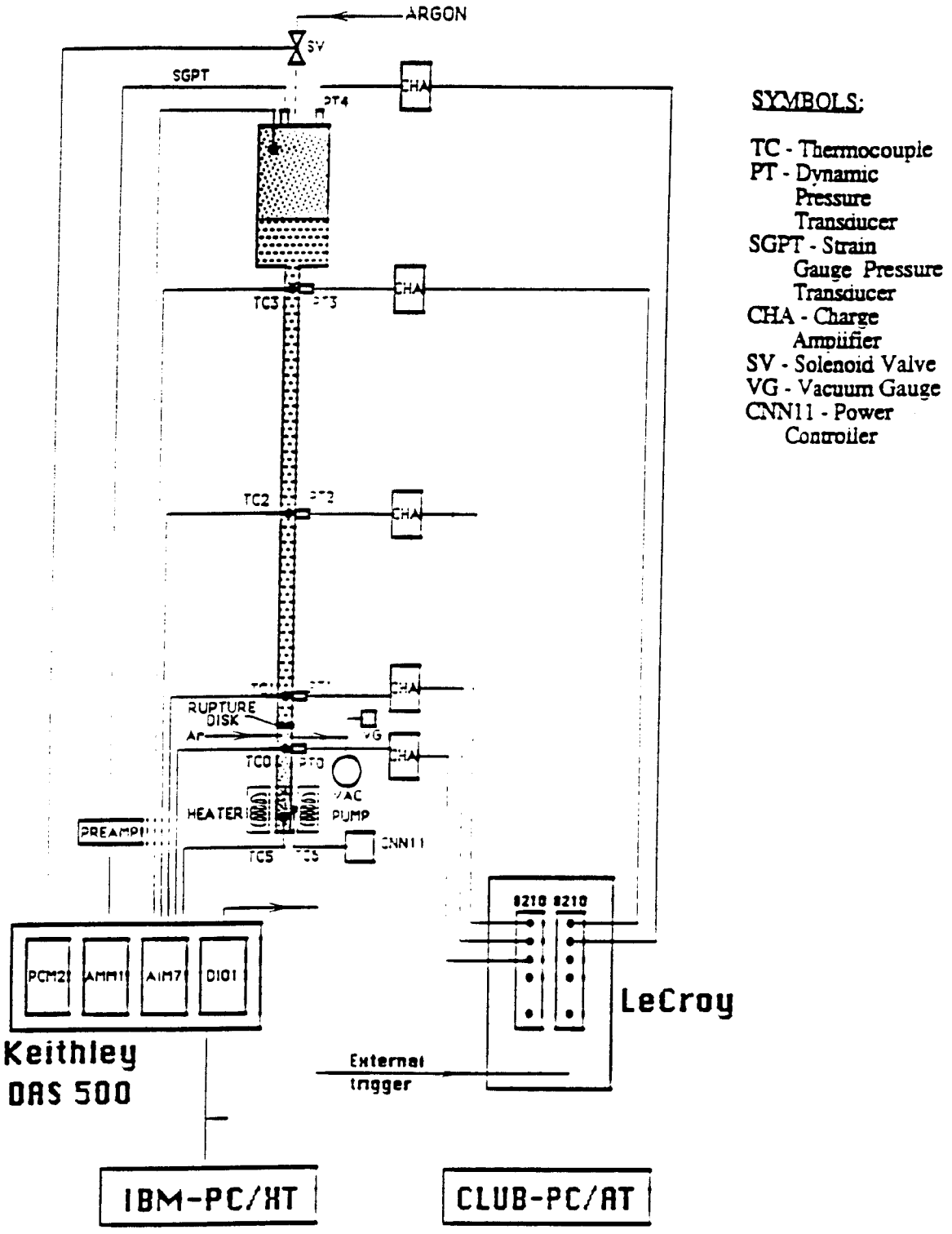

Figure 4.2: Proposed measurement and data acquisition system.

pressure transducers are placed along the shock tube to record the dynamic pressure changes. They were chosen because of their high sensitivity (pC/psi, nominal), short rise time (2μsec), and their ability to measure spikes up to 69MPa in environments where the temperature can go as high as 200°C. Charge amplifiers (Model 462A, PCB Piezotronics, Inc.) are used to amplify and convert their minute charge output into voltage signals. The sensitivity (pC/psig) and range (psig/V) should be set for each pressure transducer separately depending on the expected range of pressure spikes in each particular experiment.

A Granville-Phillips series 275 convectron vacuum gauge with a digital display is used to measure the vacuum in the gas region between the disk and the fuel surface. It can sense vacuum from 100Pa to 1bar N_2 equivalent within the 15-50°C temperature compensation range of the gauge tube. When working with gases different from N_2 and air, the appropriate true pressure vs. indicated pressure calibration curve has to be used [5].

4.2.4 Data Acquisition System

Dynamic pressure traces are recorded by LeCroy, while the rest of the data is obtained through the DAS 500 (input signals are connected to the channels on the appropriate boards) which is also involved in the experiment control. Both, LeCroy and the DAS 500, are interfaces between the components of the set-up and the personal computers (due to the incompatibility of the available software and computers and shortcomings of the purchased software it was not possible to operate both systems via only one computer; two had to be used). The IBM-PC/XT (connected to DAS 500) executes a program (written

by the experimenter) that acquires thermocouple and strain gauge pressure transducer data, operates the solenoid valve through the relay, and triggers LeCroy.

Output from the strain gauge pressure transducer is first amplified by a factor of 100 within the custom made preamplifier, and then it is led to the input channel on a Keithley Analog Memory Module 1 (AMM1). Within the AMM1 circuit the signal is additionally internally amplified with a gain of 5 so that the total gain equals 500 (therefore, the maximum strain gauge pressure transducer signal of 20mV when amplified equals the AMM1 maximum input signal of +10V).

Thermocouple board AIM7 accepts all thermocouples signals (except the heater's thermocouple, T6) and amplifies them by a factor of 100, while the TTL level signal from the input-output board DIO1 (it uses digital logic) is the external trigger for LeCroy.

Operating of the solenoid valve is done by the computer via the DAS 500 and a remote relay board (it is optoisolated from the line voltage). Solid state relay (120V AC input, 3A maximum output current) is controlled by digital logic (from Power Control Module 2 board, PCM2, in the DAS 500).

Transient pressure measurements are done by running a special software (that can communicate with LeCroy system) on a personal computer. A modular instrumentation control system that we use is called "Waveform Catalyst"[15]. It has a function library to program the instruments, acquire, process, and store data, and to display the information.

We use a LeCroy system that has the following modules:

- Model 8901A Camac to GPIB Interface. It provides GPIB access from

the CLUB-PC/AT to the Camac mainframe and its instrument modules.

- Model 1434A High Power Camac Frame,
- Model 8210 Waveform digitizer (two). It is a 10-bit analog to digital converter that can sample up to 4 inputs (± 5V full scale amplitude range) with the maximum sampling rate of 1MHz (5MHz analog bandwidth). It digitizes continuously (sensitivity is 10mV/count) and stores data into the external memory module. Model 8210 can sequentially read the memory and sort the data so that the data can be placed on the Camac dataway or reconverted to the analog form for viewing on an external scope.
- Model 8800 Memory Modules (two). It has the capacity for 32K, 10 bit words, and up to three memory modules can be used in a serial fashion.

4.3 Experimental Procedure

So far only scoping isothermal tests in distilled air/water system were done. On the other hand, the hydrogen sampling system is still in the design phase, and the next several experiments should be done with fuel/coolant systems in which there will be no chemical reaction (i.e. hydrogen will not be produced). Therefore, the procedure for the case when $Li_{17}Pb_{83}$ is a fuel and coolant is at the temperature above the ambient will be given now, without references to the hydrogen sampling assembly.

Preparation Phase

1. Fill the reaction tube with fuel and melt the fuel; let the fuel cool down (note : all this is done in a glove box),
2. Place a new rupture disc into its holder,
3. Place the appropriate strain gauge pressure transducer,
4. Turn on the electronics: personal computers, the DAS 500, LeCroy, charge amplifiers (they should be in the ground state; adjust their zero offsets; set them to the appropriate psig/V range), vacuum gauge, function generator, the power controller (set the heater maximum temperature, i.e., initial fuel temperature),
5. Start the Catalyst code,
6. Mount the reaction tube, its extension, and fuel thermocouple,
7. Mount the shock-absorber,
8. Measure the barometric pressure,
9. Circulate the coolant (its height is set to the desired value) through the driver section and the expansion vessel,
10. Circulate the water through the heat exchanger,
11. Turn the vacuum pump on, and adjust the vacuum in the gas region of the reaction chamber,
12. Purge the argon through the reaction chamber (optional),
13. Monitor temperatures and static pressure (i.e. run the code on the IBM-PC/XT),

14. Turn the heater on (i.e. set the variac to the desired voltage) and wait until the fuel reaches the desired temperature; at the same time adjust the coolant temperature (via HAAKE temperature controller),

15. When the fuel temperature reaches the desired value, turn the heater off and disconnect it from the power line (at the place where quick disconnect lugs are mounted on heater wires),

16. By this time the coolant temperature should be uniform (i.e. within the acceptable range around the chosen value) so that the valves on the coolant inlet and outlet side, as well as the valve on the sight glass side, should be now closed (manually),

17. Pressurize (operating the solenoid valve) the driver section up to the pressure close to the lower end of the standard manufacturing design range of the particular rupture disk,

18. Turn the vacuum pump off and close the valve on the line to the vacuum gauge,

19. Begin the 15sec countdown period,

20. $\sim$ 10sec prior to the final manipulation of the solenoid valve, set the pressure transducers to the OPR state and prepare LeCroy for a single external trigger.

Post-Experiment Procedure

1. Set the HAAKE's temperature regulator to the room temperature,

2. Depressurize the argon supply line,

3. When the coolant temperature is equal to or lower than 40°C decrease the pressure in the shock-tube to the ambient value; for that purpose lift the HAAKE's cover and open the water inlet valve so that gas is released through the HAAKE's inlet line,

4. Open the valve next to the sight glass,

5. Disconnect the strain gauge pressure transducer from the battery and turn the preamplifier off,

6. Turn off the charge amplifiers and the vacuum gauge display,

7. Transfer dynamic pressure transducers traces to the hard disk; back up all the data onto floppy disks,

8. Allow the heater, the fuel, and the coolant (if heated) to cool down to the ambient temperature,

9. Backup the data from the IBM-PC/XT onto floppy disks,

10. Turn LeCroy, and DAS 500 off,

11. Turn both HAAKEs off,

12. Open the valve on the water outlet side in order to empty the column (up to the valve level),

13. Remove the shock absorber,

14. Remove the fuel and heater thermocouples,

15. Remove the reaction tube and take the sample out for further analysis (chemical and size distribution),

16. Open the holder and take the ruptured disc for the visual evaluation.

4.4 Proposed Test Matrix

As mentioned earlier in this chapter, we are mainly interested in liquid metal/water, in particular $Li_{17}Pb_{83}/H_2O$, reaction experiments in a shock-tube. But, before we perform these tests we should perform scoping tests which will prove that all components of the experimental set-up work properly. Scoping tests should also give some qualitative information on the processes involved in a liquid metal/water interaction. Therefore, it is planned to do the following scoping tests for different driving pressures:

- Isothermal experiments: water/air (in the reaction tube), water/water. These experiments will be first done in a set-up with a SS reaction tube, and then they will be repeated using a transparent quartz reaction tube;

- Thermal interaction experiments in which the chemical reaction is small or nonexistent: warm water/cold water, molten tin (or other appropriate metals)/water.

In order to fulfill the proposed goals (given in section 4.1), the test matrix given in table 4.2 is proposed for $Li_{17}Pb_{83}$/water and Pb/water experiments. Molten lead/water experiments should be done because they will produce data which can be used as check values for other values (either measured or calculated) during the data analysis.

Coolant Temperatures [°C]	20–90
Fuel Temperatures [°C]	300–600
Driving Pressures [barg]	2.5, 5, 10, 15, 20

Table 4.2: The proposed test matrix

Chapter 5

Scoping Tests

In this chapter the results of the first two scoping tests will be presented and discussed.

5.1 The First Test

The purpose of the first scoping test was to check the functioning of the whole system. It was done in the isothermal conditions. Driver section and part of the expansion vessel were filled with distilled water (total height of the water column was 2.75m). The reaction chamber contained only air at ambient pressure. Therefore, prior to the experiment, the dynamic pressure transducer PTO was in the gas, PT1 and PT2 were in the water, and PT4 was in the argon region.

The parameters of the experiment are given in table 5.1.

Due to the malfunctioning of some equipment, only four dynamic pressure transducers were used (PT0, PT1, PT2, and PT4). Their signals were connected to only one transient waveform recorder. The sampling frequency was set to 4kHz via an external clock (i.e. function generator). Expecting the largest pressure spikes of several tens of bars, the range dial on the charge

Expansion Vessel	Gas	Argon
	Temperature [°C]	25.7
	Pressure [psig]	91.37
Driver Section	Liquid	Distilled H_2O
	Temperature[°C]	24
Rupture Disc	Material	Al
	Stamped burst pressure at 72°F[psig]	82.00
	Standard manufacturing design range [psig]	73 min. 86.98 max.
Reaction Chamber	Gas	Air
	Temperature[°C]	23.9
	Pressure[psia]	14.599
Barometric Pressure [psia]		14.599

Table 5.1: Parameters of the first scoping test.

amplifier was set to 200psig/V.

As described in section 4.3, the experimental procedure is based on the assumption that the rupture disk fully opens within its standard manufacturing design range. Unfortunately, in this experiment the disk barely opened at p_{dr}=76.77psig causing pressure spikes much smaller (the largest one being 23psig) than expected. Two main reasons for the rupture disk failure should be considered:

- the disk was bad — either it was not manufactured according to the specifications (e.g. our discs came with only one score although the manufacturers catalog says that they have two), or it was not tested properly,
- the disk was mishandeled.

Since we rejected the second reason right away, we had to perform a second

test to prove it. Its results are described in section 5.2.

The pressure (SGPT) measured by the strain gauge pressure transducer (at the top of the expansion vessel) vs. time is given in fig. 5.1, while dynamic pressure traces PT0, PT1, PT2, and PT4 vs. time are given in figures 5.2, 5.3, 5.4, and 5.5 respectively[1].

The Synchronization of the Data Acquisition Systems. The DAS 500 started collecting data from the strain gauge pressure transducer at the same time when LeCroy was triggered. Since LeCroy has collected 3071 pre-trigger samples, that means that with the sampling interval of 250μsec the moment when the pressure PT1 has a negative spike ($\sim$1.92sec) (which should represent the bursting of the rupture disk), corresponds to 1.152sec after the trigger. According to the strain gauge pressure transducer, the disk has ruptured at 1.170sec (see fig. 5.1). Keeping in mind that the sampling interval in strain gauge pressure transducer measurements was 30msec (maximum sampling interval imposed by the DAS 500 and the measurement setup), we conclude that the timing of both data acquisition systems is within acceptable limits.

Discussion of Data. The poor resolution of the dynamic pressure traces is the consequence of the pressure pulses of much smaller intensity than expected and the pressure range chosen before the test. Because of the incomplete rupture of the diaphragm, the hydrodynamic situation during the experiment cannot be completely understood.

The data indicates that 1.152sec after both data acquisition systems were triggered, the rupture disk "bursted". At that moment PT1 and PT2 have

[1] For the locations of the pressure transducers, see fig. 4.2 on page 63.

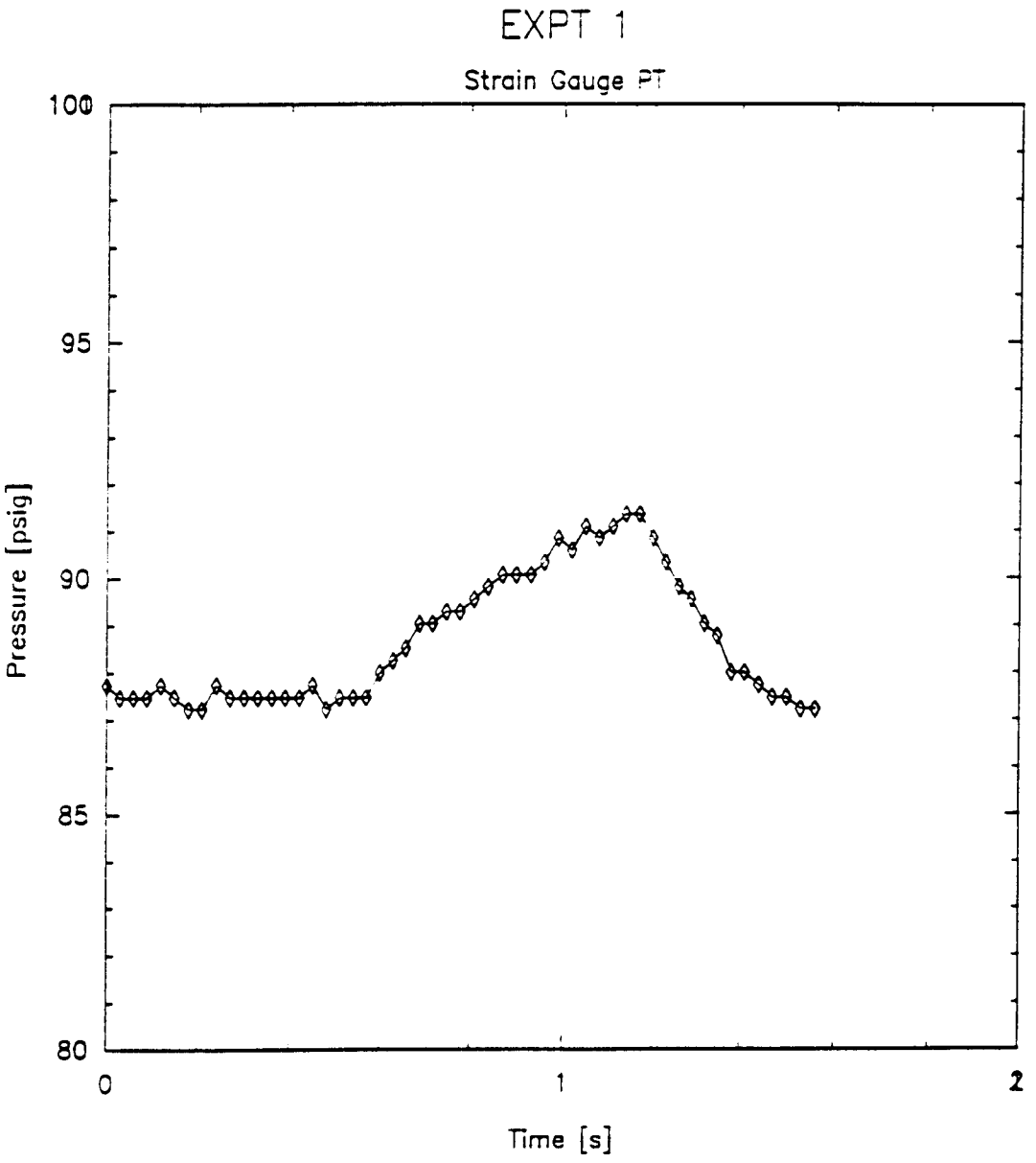

Figure 5.1: Pressure SGPT vs. time

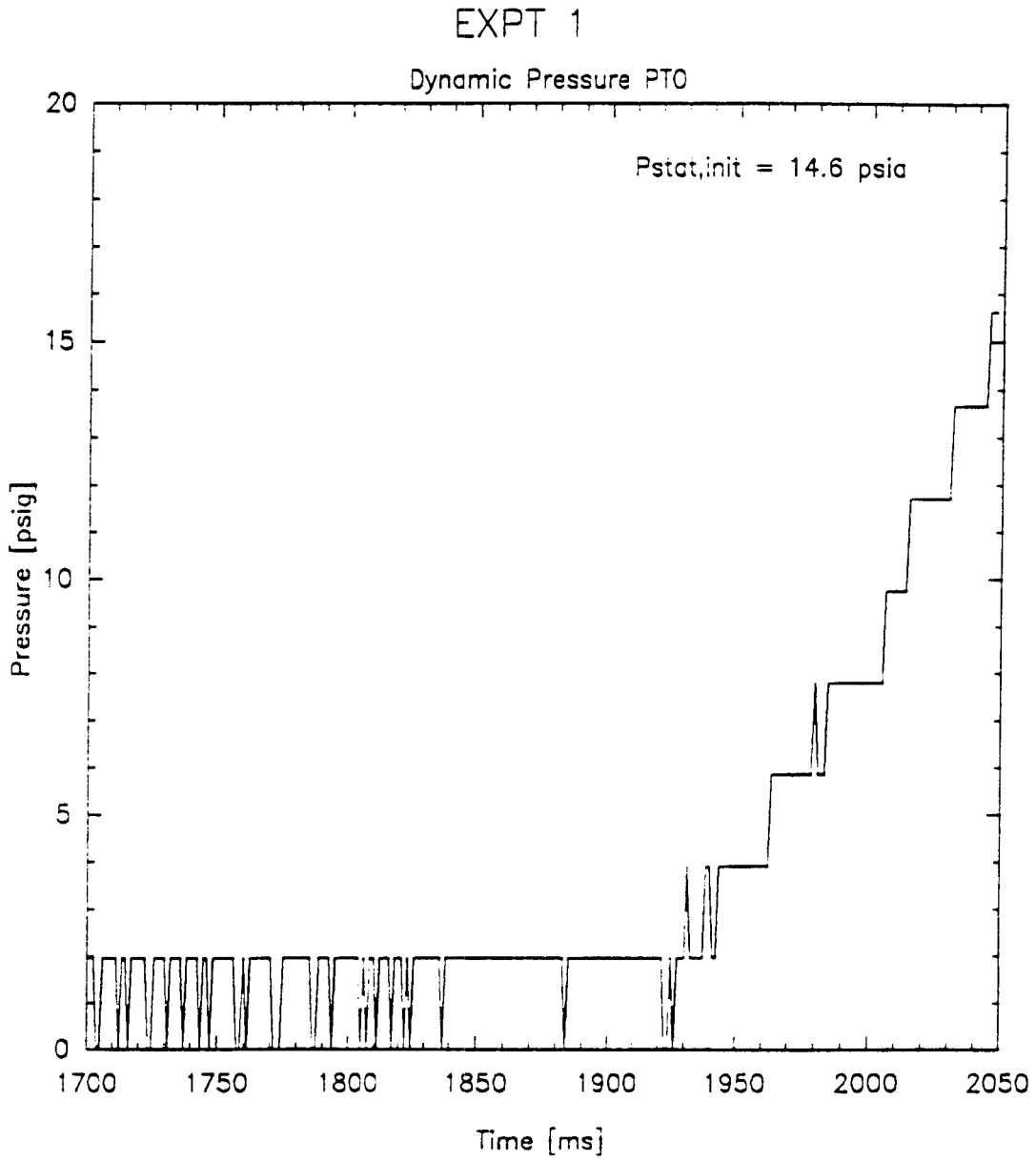

Figure 5.2: Pressure PT0 vs. time

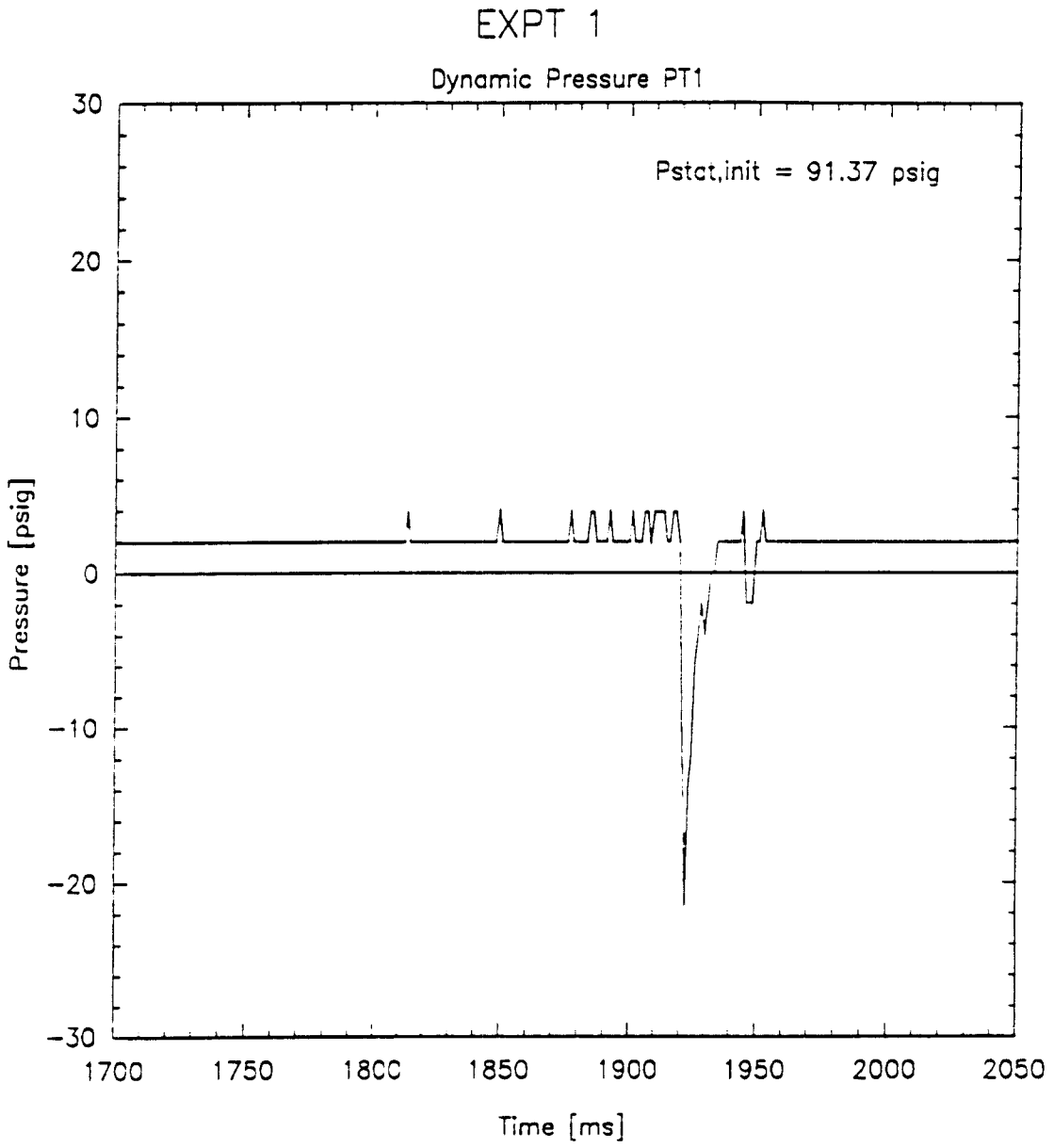

Figure 5.3: Pressure PT1 vs. time

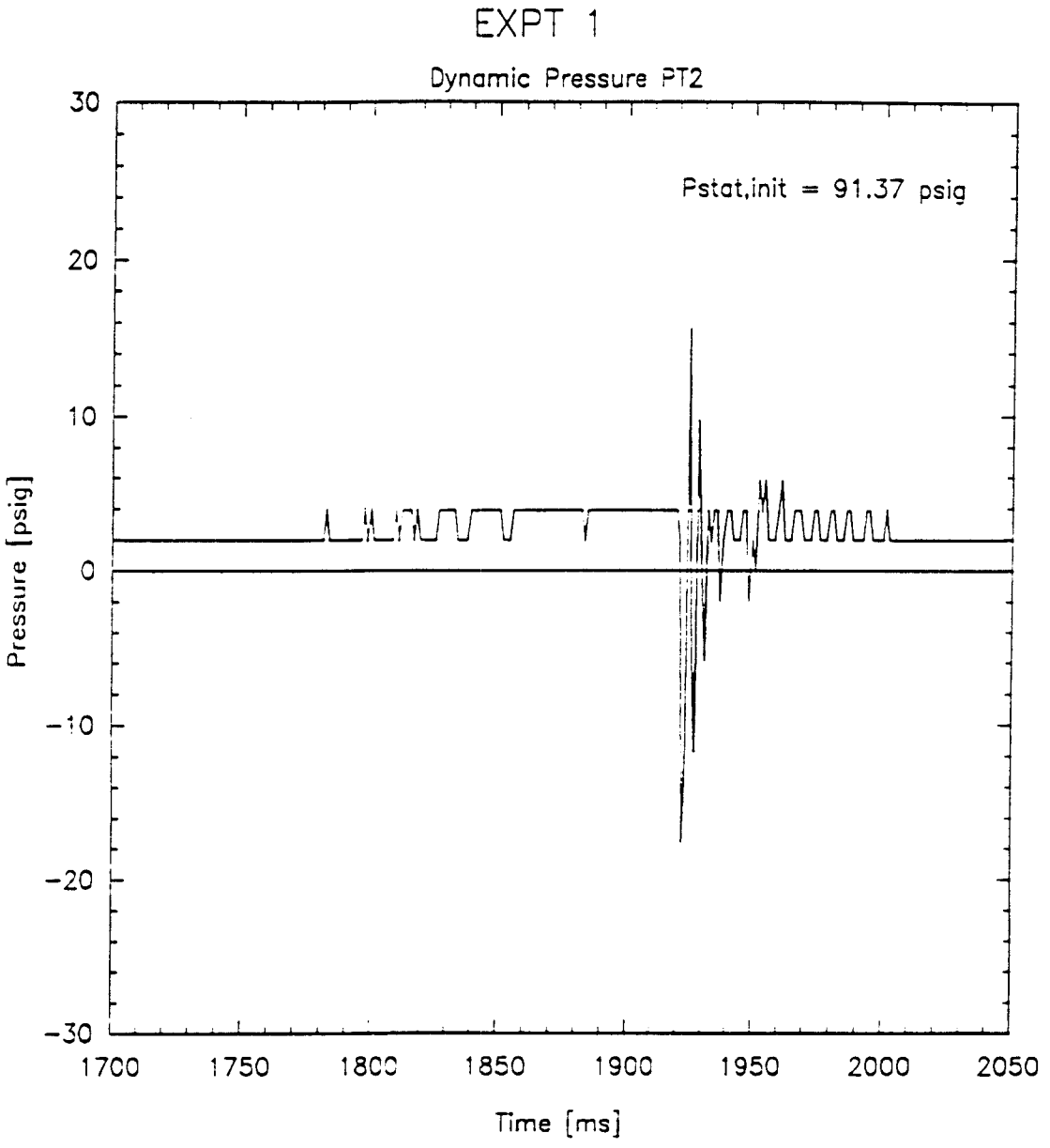

Figure 5.4: Pressure PT2 vs. time

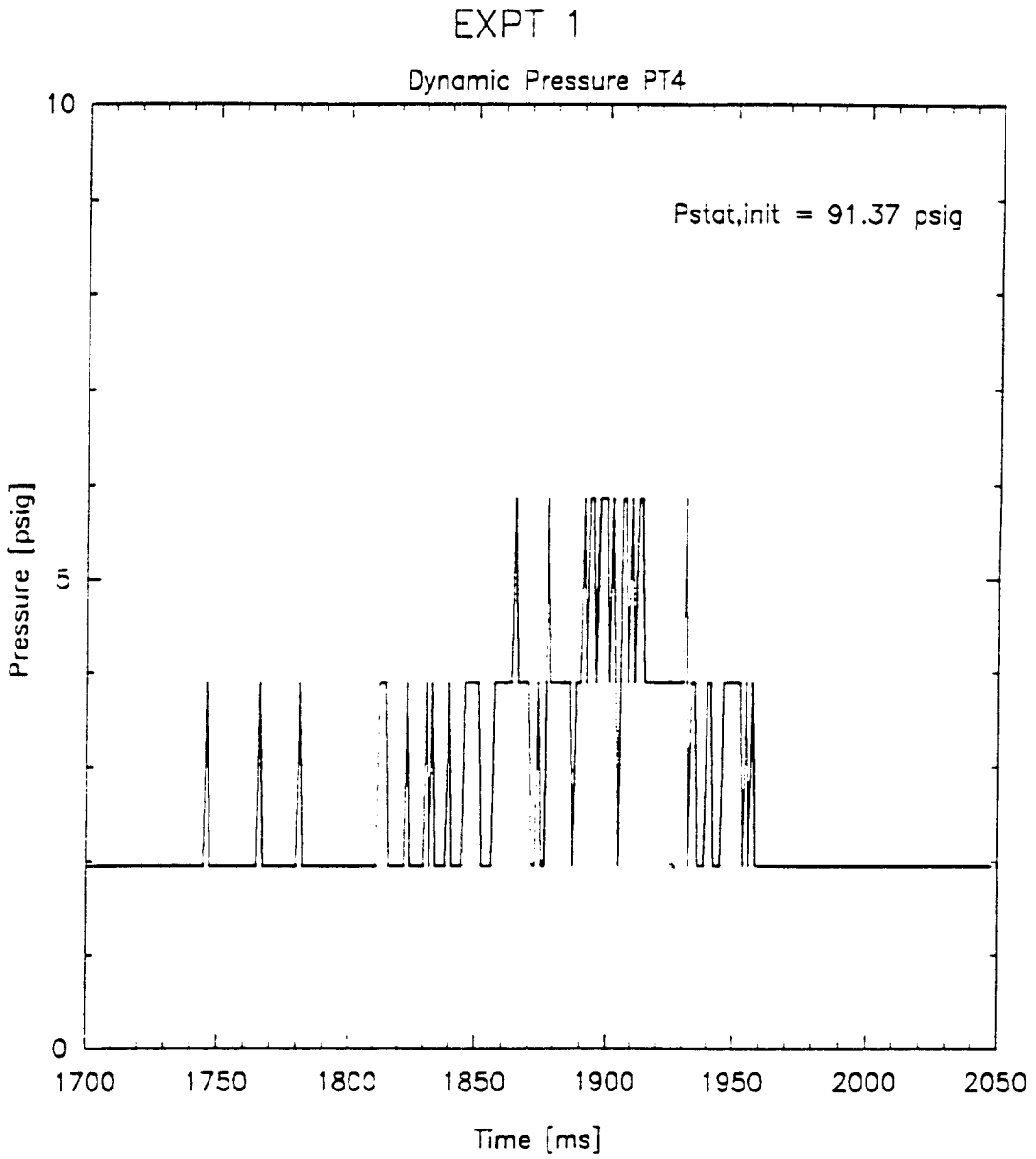

Figure 5.5: Pressure PT4 vs. time

registered an abrupt pressure decrease (negative spikes), while the pressure in the reaction chamber (PT0 trace) started to increase slowly. The delay in the response of PT4 is due to the finite time of travel of the pressure pulse along the tube.

Since the opening in the diaphragm was extremely small and water was "spraying" from the driver section into the reaction chamber, only a single long pressure spike was present in PT0 trace.

5.2 The Second Test

The second test was done with the same initial parameters as the first one, and the rupture disk was taken from the same batch. Again, the disc barely opened, in a pattern similar to the one in the first test. Unfortunately, due to an error in the experimental procedure the pressure traces were lost, so that they cannot be compared with the data from the first test.

5.3 Conclusions

These two scoping tests have demonstrated that the whole apparatus (except the rupture discs), together with the auxiliary equipment, measurement and data acquisition systems, work properly in isothermal conditions. Computers with the existing software (bought for LeCroy and written for DAS 500) are able to control and trigger the experiment. We became aware of some shortcomings of the software that can be easily overcome. Also, we realized what upgrades of the set-up should be made (e.g. to mount the additional strain

gauge pressure transducer on the argon supply line, to have extra spare fragile parts, and so on).

The process of adjusting the expansion vessel pressure to the lower limit of the standard manufacturing design range of the rupture disc, and the synchronization of the disc rupturing and the triggering of LeCroy and DAS 500 should be eventually improved. It would be the best if we could use the pressure transducer PT0 signal to trigger LeCroy.

However, the first question that needs to be resolved is the failure of the disks to rupture properly. Our approach to solve this problem will include the following:

1. Experiment with a rupture disk from a different batch (i.e., of different stamped burst pressure). The transparent quartz crucible will be used instead of the stainless steel reaction tube and the burst will be recorded on a high speed camera.

2. Experiment with the doubly scored disc that will be specially ordered from the same manufacturer (Fike Corp.).

If the disk still fails to open fully, then the use of rupture discs from a different manufacturer (e.g., PROQUIP) should be considered.

Once the problem with the disks is solved, we should proceed with our experimental plan defined in section 4.4.

References

1. P. O. Biney, S. Lomperski, M. L. Corradini, and J. Krueger. A mass transport model for hydrogen generation during lithium - lead/water interactions. Technical Report UWFDM-808, Fusion Technology Institute, UW-Madison, 1989.

2. V. Coen. Lithium lead eutectic as breeding material in fusion reactors. Invited paper to be presented at the First International Conference on Fusion Reactor Materials - Tokyo, December 3-6 1984.

3. J. G. Collier. *Convective Boiling and Condensation.* Mc Graw-Hill Book Co., second edition.

4. K. Darby, R. C. Pottinger, N. J. M. Rees, and R. G. Turner. The thermal interaction between water and molten aluminum under impact conditions in a strong tube. In *Engineering of Fast Reactors for safe and reliable operation, Vol. II.* Karlsruhe, Oct. 9-13, 1972, 1973.

5. Granville Phillips Co., USA. *Series 275 Digital Readout Convectron Vacuum Gauges, Instruction Manual,*, Aug. 1987.

6. J. P. Herzog. *Lithium-Lead/Water Reaction Experiments and Analysis.* PhD thesis, University of Wisconsin-Madison, 1987.

7. J. P. Herzog and M. L. Corradini. Lithium-lead/water reaction experiments and analysis. In *8-th Topical Meeting on the Technology of Fusion Energy, Salt Lake City, Utah, USA, October 9–13, 1988.*

8. J. P. Herzog and M.L. Corradini. Modelling of lithium-lead/water interactions in a fusion reactore design. Technical Report UWFDM-559, Fusion Technology Insititute, University of Wisconsin — Madison, September 1983. Revised August 1984.

9. J. J. Hillary, P. Curry, and L. R. Taylor. Preliminary experimental studies of the interaction of water with molten lead and molten salt mixtures. In *Engineering of Fast Reactors for safe and reliable operation, Vol II.* Karsruhe, Oct. 9-13, 1972, 1973.

10. D.W. Jeppson, L.D. Muhlestein, and S. Cohen. Fusion reactor breeder material safety compatibility studies. *Nuclear Technology/Fusion*, 4, Sept. 1983.

11. H. M. Kottowski and G. Grossi. Investigation of eutectic PbLi — water interactions in constraint geometry at variable system pressures. Technical report, Commission of the European Communities, Joint Research Center, Ispra Establishement, ISPRA (Varese), Italy, Oct. 1983.

12. O. Kranert and H. Kottowski. Small scale lithium-lead/water interaction studies. Submitted for publication in NED/Fusion, 1990.

13. Oliver Kranert. *Untersuchungen über die Thermischen und Chemischen Reaktionen von Lithium-Blei-Schmelze mit Wasser.* PhD thesis, Fakultät für Bergbau, Hüttenwesen und Geowissenschaften der Rheinisich-Westfälischen Technischen Hochschule Aaschen, 1989. in german.

14. G. Kuhlborsch and F. Reiter. Physical properties and chemical reaction behaviour of $Li_{17}Pb_{83}$ related to its use asa fusion reactor blanket material. In *Nuclear Engineering and Design/Fusion, Vol. 1*, pages 195–203, Amsterdam, 1984. North-Holland.

15. LeCroy Co., USA. *Waveform-Catalyst Ver.4.00, User's manual*, Jul 1990.

16. S. Lomperski, P. O. Biney, and M. L. Corradini. Mass transfer modelling of liquid metal/water interactions. In *13-th ANS Topical Meeting on Fusion Technology, Chicago, October 1990.*

17. S. W. Lomperski. *Molten Li/Water Interaction Experiments: Explosive Reactions and Reaction Rate Measurements.* PhD thesis, University of Wisconsin — Madison, USA, 1991.

18. M. D. Oh and M. L. Corradini. A propagation/expansion model for large scale vapor explosions. *Nuclear Science and Engineering*, 95:225–240, 1987.

19. G.C. Park and M. L. Corradini. Estimates of limits to fuel/coolant mixing. In *National Heat Transfer Conference, August 1991.*

20. S. J. Piet, D. W. Jeppson, L. D. Muhlestein, M. S. Kazimi, and M. L. Corradini. Liquid metal chemical reaction safety in fusion facilities. In *Fusion Engineering and Design, 5*, pages 273–298. North Holland, Amsterdam, 1987.

21. M. Raz. Vertical shock tube mechanical design for liquid metal/water interactions. Technical Report UWRSR69, University of Wisconsin –

Madison, Reactor Safety Research, NEEP Dept., UW – Madison, WI, March 1991.

22. A. Segev, R. E. Henry, and S. G. Bankoff. Thermal and hydrodynamic interactions in shocktube configuration. In *Topics in Two-Phase Heat Transfer and Flow.* ASME, 1978. Presented at the Winter Annual Meeting of ASME, San Francisco, CA, December 10-15, 1978.

23. A. Sharon and S. G. Bankoff. Fuel - collant interaction in a shock tube with initially - established film boiling. Technical Report -C00-2512-16, Chemichal Engineering Department, Northwestern University, Evanston, IL 60201, USA, February 1979.

24. Vacuum/Atmospheres Company, USA. *Dri-Lab HE/DL Series, Technical Manual*, DRI-LAB-08/85 edition.

25. Robert C. Weast, editor. *The CRC Handbook of Chemistry and Physics.* CRC Press, 18901 Cranwood Parway, Cleveland Oh, 55 edition, 1974.